Revista ALCONPAT
www.revistaalconpat.org
eISSN 2007-6835
Revista de la Asociación Latinoamericana de Control de Calidad, Patología y Recuperación de la Construcción

# New model for complete design of rectangular isolated footings taking into account that the contact surface works partially in compression

A. Luévanos Rojas [1]*
*Contact Author: arnulfol_2007@hotmail.com
DOI: https://doi.org/10.21041/ra.v13i2.671

Received: 21/02/2023 | Received in revised form: 13/04/2023 | Accepted: 20/04/2023 | Published: 01/05/2023

## ABSTRACT

This paper shows a new model for complete design of rectangular isolated footings under uniaxial and biaxial bending, considering that the footing area in contact with the soil partially works to compression. The methodology is presented by integration to obtain moments, flexural shearing and punching shearing. Numerical examples are presented for design of rectangular isolated footings under uniaxial and biaxial flexion and are compared with the current model (total area works in compression) in terms of concrete and steel volumes. The current model shows greater volumes of concrete and steel. Therefore, the new model is the most appropriate, since it presents better quality control in the resources used.
**Keywords:** rectangular isolated footings; new model for complete design; moments; flexural shearing; punching shearing.

**Cite as:** Luévanos Rojas, A. (2023), *"New model for complete design of rectangular isolated footings taking into account that the contact surface works partially in compression"*, Revista ALCONPAT, 13 (2), pp. 192 – 219, DOI: https://doi.org/10.21041/ra.v13i2.671

[1] Instituto de Investigaciones Multidisciplinarias, Universidad Autónoma de Coahuila, Torreón, Coahuila, México.

**Contribution of each author**
In this work there was only one author.



**Discussions and subsequent corrections to the publication**
Any dispute, including the replies of the authors, will be published in the first issue of 2024 provided that the information is received before the closing of the third issue of 2023.

# Nuevo modelo para el diseño completo de zapatas aisladas rectangulares tomando en cuenta que la superficie de contacto funciona parcialmente en compresión


## RESUMEN

Este documento muestra un nuevo modelo para diseño completo de zapatas aisladas rectangulares bajo flexión uniaxial y biaxial, tomando en cuenta que el área de la zapata en contacto con el suelo funciona parcialmente a compresión. La metodología se presenta por integración para obtener momentos, cortantes por flexión y penetración. Los ejemplos numéricos se presentan para el diseño de zapatas aisladas rectangulares bajo flexión uniaxial y biaxial, y se comparan con el modelo actual (área total funciona en compresión) en términos de volúmenes de concreto y acero. El modelo actual muestra mayores volúmenes de concreto y acero. Por lo tanto, el nuevo modelo es el más adecuado, ya que presenta mejor control de calidad en los recursos utilizados.


**Palabras clave:** zapatas aisladas rectangulares; nuevo modelo para diseño completo; momentos; cortante por flexión; cortante por penetración.


# Um novo modelo para o dimensionamento completo de fundações isoladas retangulares levando em consideração que a superfície de contato funciona parcialmente em compressão


## RESUMO

Este artigo mostra um novo modelo para o dimensionamento completo de fundações isoladas retangulares sob flexão uniaxial e biaxial, levando em consideração que a área da sapata em contato com o solo funciona parcialmente à compressão. A metodologia é apresentada por integração para obter momentos, cisalhamento por flexão e punção. Exemplos numéricos são apresentados para o projeto de fundações isoladas retangulares sob flexão uniaxial e biaxial e são comparados ao modelo atual (a área total funciona em compressão) em termos de volumes de concreto e aço. O modelo atual mostra maiores volumes de concreto e aço. Portanto, o novo modelo é o mais apropriado, pois apresenta melhor controle de qualidade nos recursos utilizados.


**Palavras-chave**: fundações isoladas retangulares; novo modelo para dimensionamento completo; momentos; cisalhamento de flexão; punção.



**Legal Information**

Revista ALCONPAT is a quarterly publication by the Asociación Latinoamericana de Control de Calidad, Patología y Recuperación de la Construcción, Internacional, A.C., Km. 6 antigua carretera a Progreso, Mérida, Yucatán, 97310, Tel.5219997385893, alconpat.int@gmail.com, Website: www.alconpat.org

Reservation of rights for exclusive use No.04-2013-011717330300-203, and ISSN 2007-6835, both granted by the Instituto Nacional de Derecho de Autor. Responsible editor: Pedro Castro Borges, Ph.D. Responsible for the last update of this issue, Informatics Unit ALCONPAT, Elizabeth Sabido Maldonado.

The views of the authors do not necessarily reflect the position of the editor.

# 1. INTRODUCTION

The design of shallow footings supported on the ground depends of the loads and moments provided by the columns.
Figure 1 shows the distribution of soil pressure under the rigid footing that depends on the type of soil, and the position of the applied resultant force at the center of gravity of the base. Figure 1(a) presents a footing resting on sandy soil. Figure 1(b) shows a footing resting on clay soil. Figure 1(c) presents the uniform soil pressure distribution used in the current design.
The bearing capacity has been investigated for shallow footings subjected to biaxial bending, which takes into account a linear ground pressure distribution and this contact area works partly in compression (Irles-Más and Irles-Más, 1992; Özmen, 2011; Rodriguez-Gutierrez and Aristizabal-Ochoa, 2013a, b; Lee et al., 2015; Kaur and Kumar, 2016; Bezmalinovic Colleoni, 2016; Dagdeviren, 2016; Aydogdu, 2016; Girgin, 2017; Turedi et al., 2019; Al-Gahtani and Adekunle, 2019; Galvis and Smith-Pardo, 2020; Rawat et al., 2020; Lezgy-Nazargah et al., 2022; Gör, 2022).

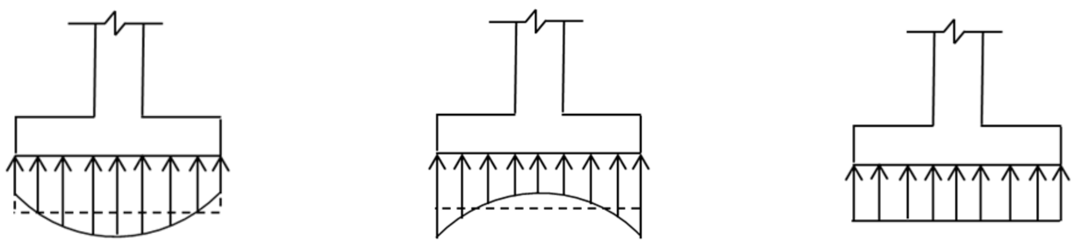

(a) (b) (c)

Figure 1. Pressure distribution under the footing
Source: Own elaboration

The mathematical models for the foundations design: for isolated footings have been developed for square, circular and rectangular shapes (Algin, 2000, 2007; Luévanos-Rojas, 2012a, b, 2013, 2014a, 2015a; Luévanos-Rojas et al., 2013, 2014b, 2016b, et al., 2017; Filho et al., 2017; López-Chavarría et al., 2017a, c, 2019; Khajehzadeh et al., 2014); For rectangular, trapezoidal, corner, T-shaped and strap combined footings (Jahanandish et al., 2012; Luévanos-Rojas, 2014c, 2015b, c, d, 2016[a], b, et al., 2018a, b, 2020; López-Chavarría et al., 2017b; Velázquez-Santillán et al., 2019; Aguilera-Mancilla et al., 2019; Yáñez-Palafox et al., 2019). These papers take into account the entire contact area working under compression.
The models closest to this document are: Soto-García et al. (2022) proposed a mathematical model to obtain the minimum area for circular isolated footings, taking into account that footing area in contact with the soil works partially to compression, this model presents a case because the analysis is developed for the resultant moment. Vela-Moreno et al. (2022) developed a mathematical model to find the minimum surface for rectangular isolated footings, taking into account that footing area in contact with the soil works partially to compression, this model shows five cases for biaxial bending, two cases for uniaxial bending (Load is on the X axis) and another two cases for uniaxial bending (Load is on the Y axis). Kim-Sánchez et al. (2022) presented a mathematical model to obtain the thickness and the areas of transverse and longitudinal steel for circular isolated footings, taking into account that footing area in contact with the soil works partially to compression.
This investigation presents a new analytical model to obtain a complete design (thickness and areas of transverse and longitudinal steel) for rectangular isolated footings, taking into account that footing area in contact with the soil works partially to compression, this model is based on the area of contact with the soil (sides of footing) of the model proposed by Vela-Moreno *et al.* (2022). The formulation of the new model is developed by integration to find the moments, the flexural shearing

and the punching shearing under the code criteria (ACI 318S-19). Other authors present the equations to find the complete design of a rectangular isolated footing, but considering the total surface working under compression. Numerical examples are shown to find the complete design of rectangular isolated footings under axial load and moments in one and two directions and the results are compared with those of other authors to observe the differences. The ground contact areas presented in this document are based on the work proposed by Vela-Moreno et al. (2022). This model will have its impact on the construction industry with lower costs (materials and labor).

## 2. FORMULATION OF THE NEW MODEL

A rigid rectangular isolated footing is deformed in a planar shape, i.e., the distribution of soil pressure under the footing is considered linear.
The general equation for any footings subjected to biaxial bending under a factorized axial load and two factorized orthogonal moments is:

$$\sigma_u(x,y) = \frac{P_u}{h_x h_y} + \frac{12 M_{ux} y}{h_x {h_y}^3} + \frac{12 M_{uy} x}{{h_x}^3 h_y} \tag{1}$$

where: $\sigma_u$ is the factorized pressure generated by the soil due to the factorized axial load and the factorized moments that are applied at the footing, $P_u$ is the factorized axial load, $M_{ux}$ is the factorized moment on the X axis, $M_{uy}$ is the factorized moment on the Y axis, $h_x$ and $h_y$ are the sides of the footing, $x$ and $y$ are the coordinates where the pressure generated by the soil is located. The biaxial bending equation can be applied when the resultant force $P_u$ is located inside the central nucleus (area working fully in compression), and when the resultant force $P_u$ is outside of the central nucleus (area working partially in compression) is not valid.
When the resultant force $P_u$ is outside of the central nucleus, the general equations of soil pressure under the footing subjected to uniaxial and biaxial bending are:
Uniaxial bending ($P_u$ is located on the Y axis):

$$\sigma_z(x,y) = \frac{\sigma_{umax}\left(2h_{y1} - h_y + 2y\right)}{2h_{y1}} \tag{2}$$

Uniaxial bending ($P_u$ is located on the X axis):

$$\sigma_z(x,y) = \frac{\sigma_{umax}(2h_{x1} - h_x + 2x)}{2h_{x1}} \tag{3}$$

Biaxial bending:

$$\sigma_z(x,y) = \frac{\sigma_{umax}\left[h_{y1}(2x - h_x) + h_{x1}\left(2y - h_y\right) + 2h_{x1}h_{y1}\right]}{2h_{x1}h_{y1}} \tag{4}$$

where: $\sigma_{umax}$ is the factorized maximum pressure generated by the soil due to the factorized axial load and the factorized moments that are applied at the footing.
The critical sections for moments are located on the *a-a* and *b-b* axes, for the critical sections for the flexural shearing are located on the *c-c* and *e-e* axes, and the critical section for the punching shearing occurs in the perimeter formed by points 5, 6, 7 and 8 (ACI 318S-19).

## 2.1. Rectangular isolated footing subjected to uniaxial bending

Figure 2 shows the four possible cases to obtain the minimum area of a rectangular isolated footing subjected to uniaxial bending. Two cases when *P* is located on the Y axis: 1) when *P* is located inside the central nucleus; 2) when *P* is located outside the central nucleus. Two cases when *P* is located on the X axis: 1) when *P* is located inside the central nucleus; 2) when *P* is located outside the central nucleus.

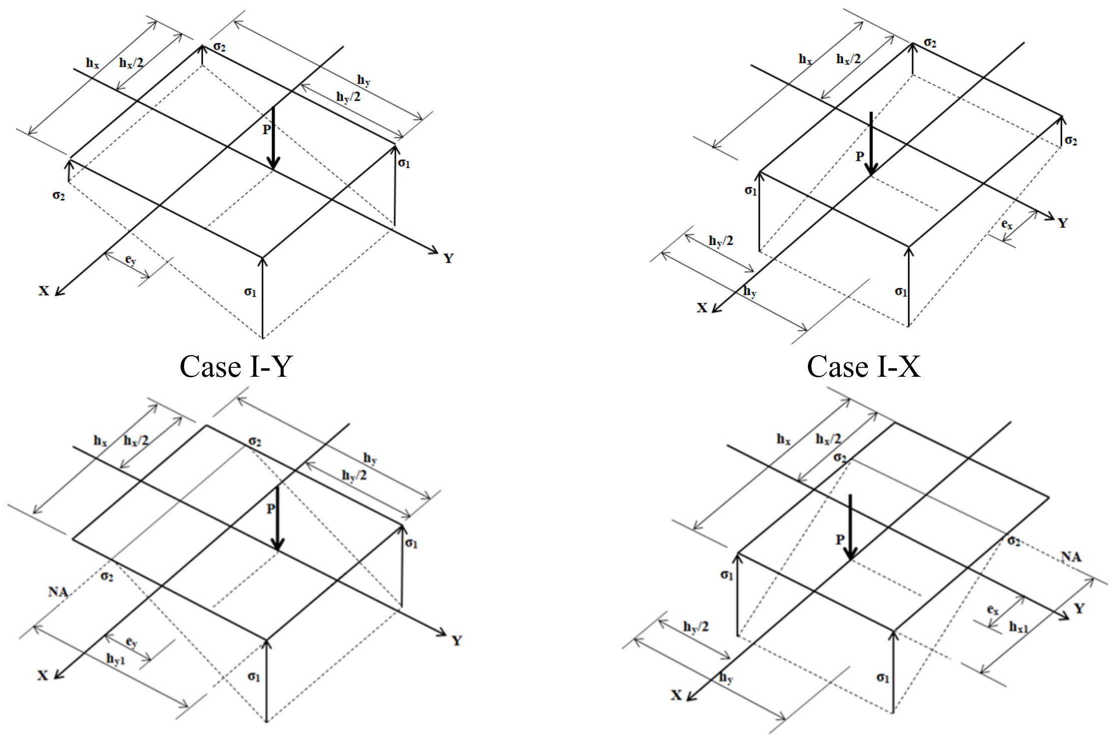


Case I-Y Case I-X

Case II-Y Case II-X

Figure 2. Four possible cases of minimum area for uniaxial bending
Source: Own elaboration based on Vela-Moreno et al. (2022)

Figure 3 shows the critical sections for moments and flexural shearing of four possible cases: Case I-Y when *P* is located on the Y axis, and inside the central nucleus. Case II-Y when *P* is located on the Y axis, and outside the central nucleus: Case II-YA when the neutral axis is located $h_y/2 - h_{y1} \geq c_1/2$ (moment) and $h_y/2 - h_{y1} \geq c_1/2 + d$ (flexural shearing); Case II-YB when the neutral axis is located $h_y/2 - h_{y1} \leq c_1/2$ (moment) and $h_y/2 - h_{y1} \leq c_1/2 + d$ (flexural shearing). Case I-X when *P* is located on the X axis, and inside the central nucleus. Case II-X when *P* is located on the X axis, and outside the central nucleus: Case II-XA when the neutral axis is located $h_x/2 - h_{x1} \geq c_2/2$ (moment) and $h_x/2 - h_{x1} \geq c_2/2 + d$ (flexural shearing); Case II-XB when the neutral axis is located $h_x/2 - h_{x1} \leq c_2/2$ (moment) and $h_x/2 - h_{x1} \leq c_2/2 + d$ (flexural shearing).

### *2.1.1. Flexural shearing and moments*

The general equations in the “c” and “e” axes for the factored flexural shearing “$V_{uc}$” and “$V_{ue}$”, and in the “a” and “b” axes for the factored moments “$M_{ua}$” and “$M_{ub}$” are:

**Case I-Y**

$$V_{uc} = \int_{\frac{c_1}{2}+d}^{\frac{h_y}{2}} \int_{-\frac{h_x}{2}}^{\frac{h_x}{2}} \sigma_u(x, y)dxdy \tag{5}$$

$$V_{ue} = \int_{\frac{c_2}{2}+d}^{\frac{h_x}{2}} \int_{-\frac{h_y}{2}}^{\frac{h_y}{2}} \sigma_u(x,y)\,dy\,dx \tag{6}$$

$$M_{ua} = \int_{\frac{c_1}{2}}^{\frac{h_y}{2}} \int_{-\frac{h_x}{2}}^{\frac{h_x}{2}} \sigma_u(x,y)\left(y - \frac{c_1}{2}\right) dx\,dy \tag{7}$$

$$M_{ub} = \int_{\frac{c_2}{2}}^{\frac{h_x}{2}} \int_{-\frac{h_y}{2}}^{\frac{h_y}{2}} \sigma_u(x,y)\left(x - \frac{c_2}{2}\right) dy\,dx \tag{8}$$

where: $d$ is the effective depth of the footing, $c_1$ and $c_2$ are the sides of the column.
Note: Equation (1) is substituted into equations (5) to (8) and $M_{uy}$ = 0 and the integrals are developed to obtain the final equations.

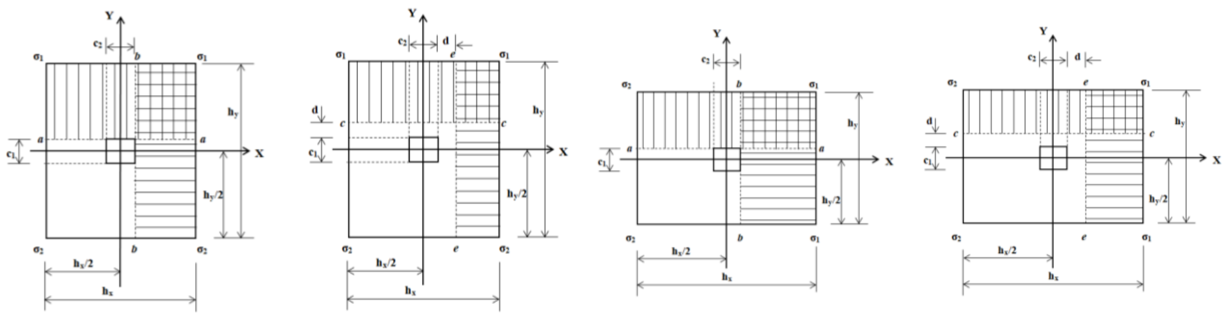

Case I-Y Case I-X

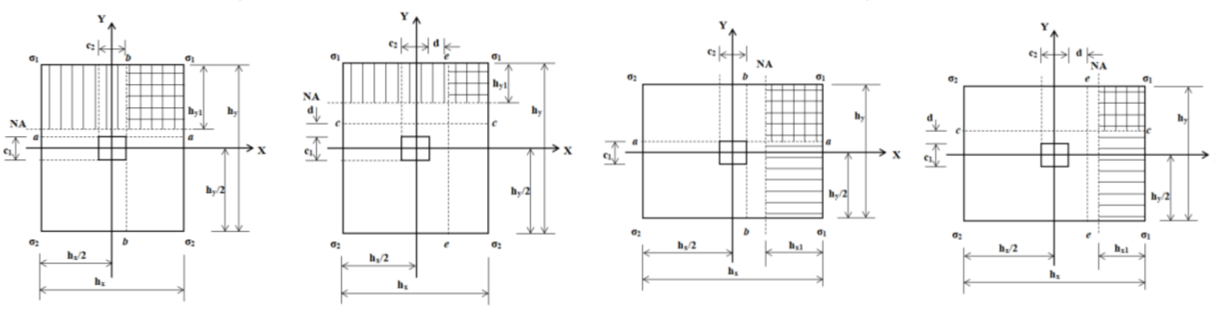

Case II-YA Case II-XA

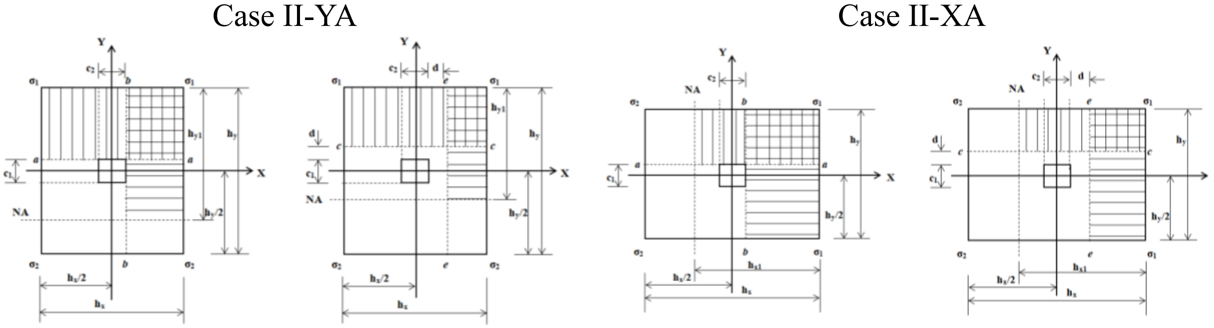

Case II-YB Case II-XB

Moments Flexural shearing Moments Flexural shearing

Figure 3. Moments and flexural shearing for uniaxial bending

Source: Own elaboration

**Case II-YA**

For $h_y/2 - h_{y1} \geq c_1/2 + d$ (flexural shearing) and $h_y/2 - h_{y1} \geq c_1/2$ (moment) are:

$$V_{uc} = \int_{\frac{h_y}{2}-h_{y1}}^{\frac{h_y}{2}} \int_{-\frac{h_x}{2}}^{\frac{h_x}{2}} \sigma_z(x,y)dxdy \tag{9}$$

$$V_{ue} = \int_{\frac{c_2}{2}+d}^{\frac{h_x}{2}} \int_{\frac{h_y}{2}-h_{y1}}^{\frac{h_y}{2}} \sigma_z(x,y)dydx \tag{10}$$

$$M_{ua} = \int_{\frac{h_y}{2}-h_{y1}}^{\frac{h_y}{2}} \int_{-\frac{h_x}{2}}^{\frac{h_x}{2}} \sigma_z(x,y)\left(y - \frac{c_1}{2}\right)dxdy \tag{11}$$

$$M_{ub} = \int_{\frac{c_2}{2}}^{\frac{h_x}{2}} \int_{\frac{h_y}{2}-h_{y1}}^{\frac{h_y}{2}} \sigma_z(x,y)\left(x - \frac{c_2}{2}\right)dydx \tag{12}$$

**Case II-YB**

For $h_y/2 - h_{y1} \leq c_1/2 + d$ (flexural shearing) and $h_y/2 - h_{y1} \leq c_1/2$ (moment) are:

$$V_{uc} = \int_{\frac{c_1}{2}+d}^{\frac{h_y}{2}} \int_{-\frac{h_x}{2}}^{\frac{h_x}{2}} \sigma_z(x,y)dxdy \tag{13}$$

$$V_{ue} = \int_{\frac{c_2}{2}+d}^{\frac{h_x}{2}} \int_{\frac{h_y}{2}-h_{y1}}^{\frac{h_y}{2}} \sigma_z(x,y)dydx \tag{14}$$

$$M_{ua} = \int_{\frac{c_1}{2}}^{\frac{h_y}{2}} \int_{-\frac{h_x}{2}}^{\frac{h_x}{2}} \sigma_z(x,y)\left(y - \frac{c_1}{2}\right)dxdy \tag{15}$$

$$M_{ub} = \int_{\frac{c_2}{2}}^{\frac{h_x}{2}} \int_{\frac{h_y}{2}-h_{y1}}^{\frac{h_y}{2}} \sigma_z(x,y)\left(x - \frac{c_2}{2}\right)dydx \tag{16}$$

Note: Equation (2) is substituted into equations (9) to (16) and the integrals are developed to obtain the final equations.

**Case I-X**

The general equations in the "c" and "e" axes for the factored flexural shearing "$V_{uc}$" and "$V_{ue}$", and in the "a" and "b" axes for the factored moments "$M_{ua}$" and "$M_{ub}$" are equations (5) to (8). But in these equations $M_{ux}$ = 0 is substituted and the integrals are developed to obtain the final equations.

**Case II-XA**

For $h_x/2 - h_{x1} \geq c_2/2 + d$ (flexural shearing) and $h_x/2 - h_{x1} \geq c_2/2$ (moment) are:

$$V_{uc} = \int_{\frac{c_1}{2}+d}^{\frac{h_y}{2}} \int_{\frac{h_x}{2}-h_{x1}}^{\frac{h_x}{2}} \sigma_z(x,y)dxdy \tag{17}$$

$$V_{ue} = \int_{\frac{h_x}{2}-h_{x1}}^{\frac{h_x}{2}} \int_{-\frac{h_y}{2}}^{\frac{h_y}{2}} \sigma_z(x,y)dydx \tag{18}$$

$$M_{ua} = \int_{\frac{c_1}{2}}^{\frac{h_y}{2}} \int_{\frac{h_x}{2}-h_{x1}}^{\frac{h_x}{2}} \sigma_z(x,y)\left(y - \frac{c_1}{2}\right)dxdy \tag{19}$$

$$M_{ub} = \int_{\frac{h_x}{2}-h_{x1}}^{\frac{h_x}{2}} \int_{-\frac{h_y}{2}}^{\frac{h_y}{2}} \sigma_z(x,y)\left(x - \frac{c_2}{2}\right)dydx \tag{20}$$

**Case II-XB**

For $h_x/2 - h_{x1} \leq c_2/2 + d$ (flexural shearing) and $h_x/2 - h_{x1} \leq c_2/2$ (moment) are:

$$V_{uc} = \int_{\frac{c_1}{2}+d}^{\frac{h_y}{2}} \int_{\frac{h_x}{2}-h_{x1}}^{\frac{h_x}{2}} \sigma_z(x,y)dxdy \tag{21}$$

$$V_{ue} = \int_{\frac{c_2}{2}+d}^{\frac{h_x}{2}} \int_{-\frac{h_y}{2}}^{\frac{h_y}{2}} \sigma_z(x,y)dydx \tag{22}$$

$$M_{ua} = \int_{\frac{c_1}{2}}^{\frac{h_y}{2}} \int_{\frac{h_x}{2}-h_{x1}}^{\frac{h_x}{2}} \sigma_z(x,y)\left(y - \frac{c_1}{2}\right)dxdy \tag{23}$$

$$M_{ub} = \int_{\frac{c_2}{2}}^{\frac{h_x}{2}} \int_{\frac{h_y}{2}-h_{y1}}^{\frac{h_y}{2}} \sigma_z(x,y)\left(x - \frac{c_2}{2}\right)dydx \tag{24}$$

Note: Equation (3) is substituted into equations (17) to (24) and the integrals are developed to obtain the final equations.

### *2.1.2. Punching shearing*

Figure 4 shows the critical sections for punching shearing of four possible cases: Case I-Y when $P$ is located on the Y axis and inside the central nucleus. Case II-Y when P is located on the Y axis and outside the central nucleus: Case II-YA when the neutral axis is localized $h_y/2 - h_{y1} \geq c_1/2 + d/2$, Case II-YB when the neutral axis is localized $h_y/2 - h_{y1} \leq c_1/2 + d/2$. Case I-X when $P$ is located on the X axis and inside the central nucleus. Case II-X when P is located on the X axis and outside the central nucleus: Case II-XA when the neutral axis is localized $h_x/2 - h_{x1} \geq c_2/2 + d/2$, Case II-XB when the neutral axis is localized $h_x/2 - h_{x1} \leq c_2/2 + d/2$.

The general equation for the factorized punching shearing “$V_{up}$” is:

**Case I-Y**

$$V_{up} = P_u - \int_{-\frac{c_1}{2}-\frac{d}{2}}^{\frac{c_1}{2}+\frac{d}{2}} \int_{-\frac{c_2}{2}-\frac{d}{2}}^{\frac{c_2}{2}+\frac{d}{2}} \sigma_u(x,y)dxdy \tag{25}$$

Note: Equation (1) is substituted into equation (25) and $M_{uy} = 0$ and the integral is developed to obtain the final equation.

**Case II-YA**
For $h_y/2 - h_{y1} \geq c_1/2 + d/2$ is:

$$V_{up} = P_u \tag{26}$$

**Case II-YB**
For $h_y/2 - h_{y1} \leq c_1/2 + d/2$ is:

$$V_{up} = P_u - \int_{y_s}^{\frac{c_1}{2}+\frac{d}{2}} \int_{-\frac{c_2}{2}-\frac{d}{2}}^{\frac{c_2}{2}+\frac{d}{2}} \sigma_z(x,y)dxdy \tag{27}$$

where: $-c_1/2 - d/2 \leq y_s \leq c_1/2 + d/2$
Note: Equation (2) is substituted into equation (27) and the integral is developed to obtain the final equation.

**Case I-X**
Equation (1) is substituted into equation (25) and $M_{ux} = 0$ and the integral is developed to obtain the final equation.

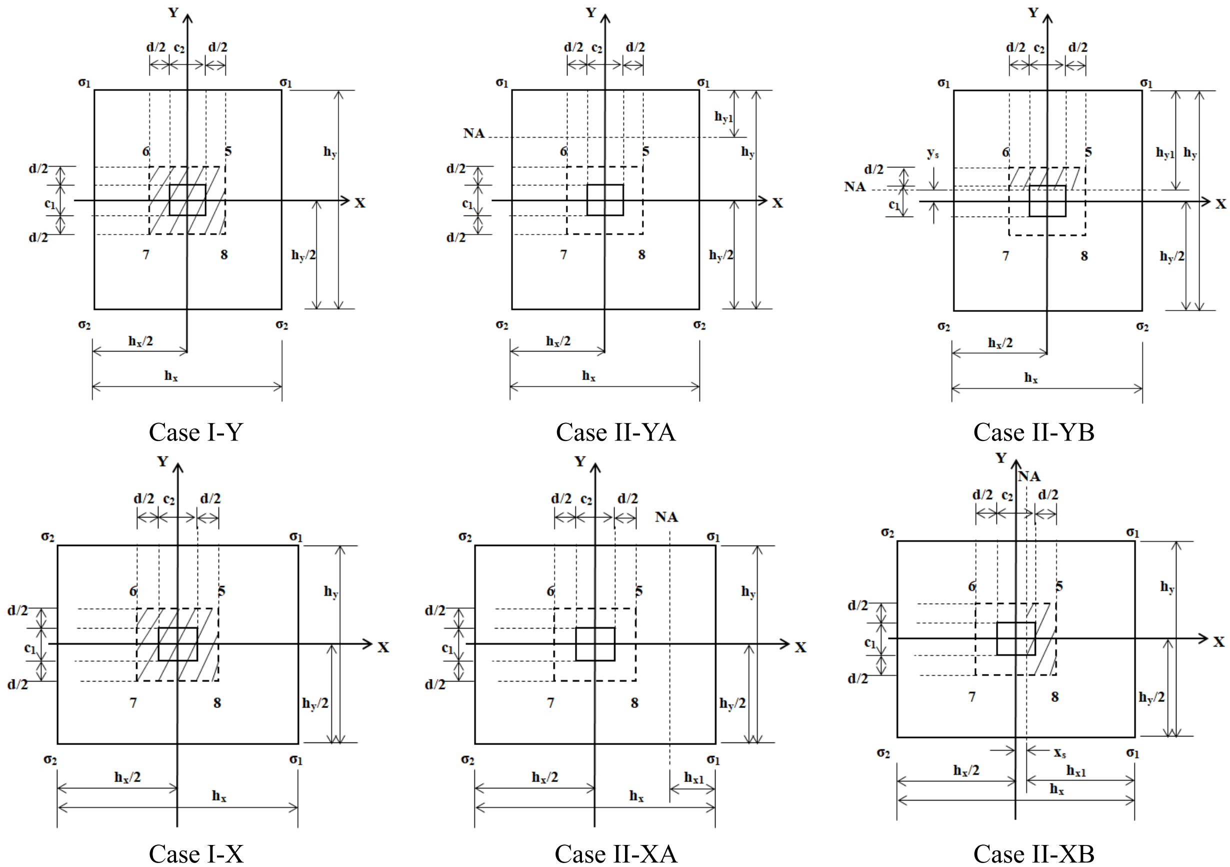


Figure 4. Punching shearing for uniaxial bending
Source: Own elaboration

**Case II-XA**
For $h_x/2 - h_{x1} \geq c_2/2 + d/2$ is equation (26).

**Case II-XB**
For $h_x/2 - h_{x1} \leq c_2/2 + d/2$ is:

$$V_{up} = P_u - \int_{x_s}^{\frac{c_2}{2}+\frac{d}{2}} \int_{-\frac{c_1}{2}-\frac{d}{2}}^{\frac{c_1}{2}+\frac{d}{2}} \sigma_z(x,y)\,dy\,dx \qquad (28)$$

where: $-c_2/2 - d/2 \leq x_s \leq c_2/2 + d/2$.
Note: Equation (3) is substituted into equation (28) and the integral is developed to obtain the final equation.

## 2.2. Rectangular isolated footing subjected to biaxial bending

Figure 5 shows the five possible cases to obtain the minimum area of a rectangular isolated footing subjected to biaxial bending.
For case I, it is considered that the total surface of the footing works under compression. The pressure generated by the soil on the footing is obtained by equation (1) (biaxial bending).
For cases II, III, IV and V consider that the total surface of the footing works partially under compression, i.e., part of the surface has zero pressure. The pressure generated by the soil on the footing is obtained by equation (4).

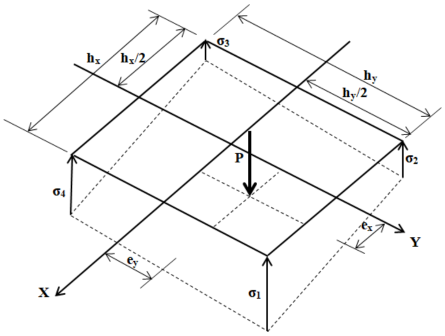


Case I

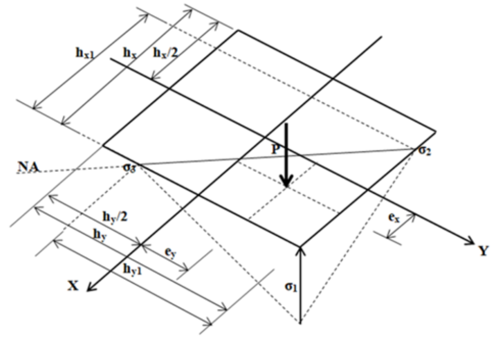


Case II

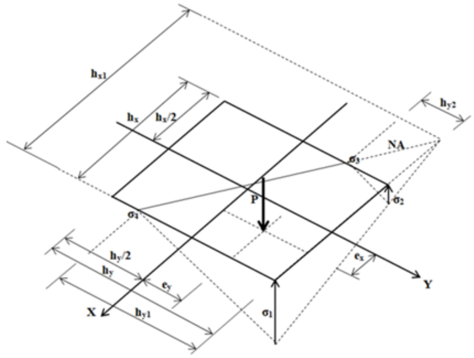


Case III

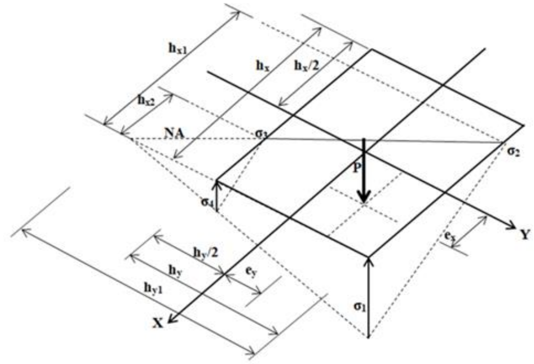


Case IV

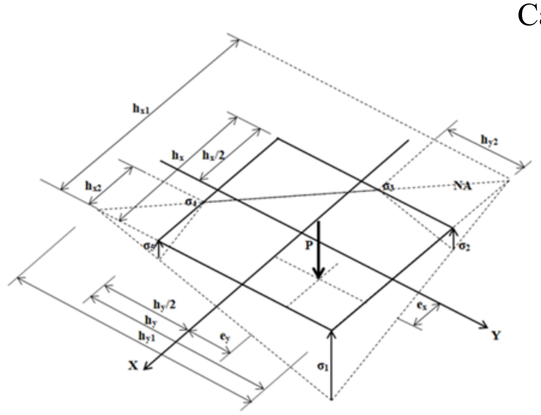


Case V

Figure 5. Five possible cases of minimum area for biaxial bending
Source: Own elaboration based on Vela-Moreno et al. (2022)

### *2.2.1. Flexural shearing and moments*

Figure 6 shows the critical sections for flexural shearing and moments for all possible cases. The general equations on the "*c*" and "*e*" axes for the factorized flexural shearing "$V_{uc}$" and "$V_{ue}$", on the "*a*" and "*b*" axes for the factorized moments "$M_{ua}$" and "$M_{ub}$" are:

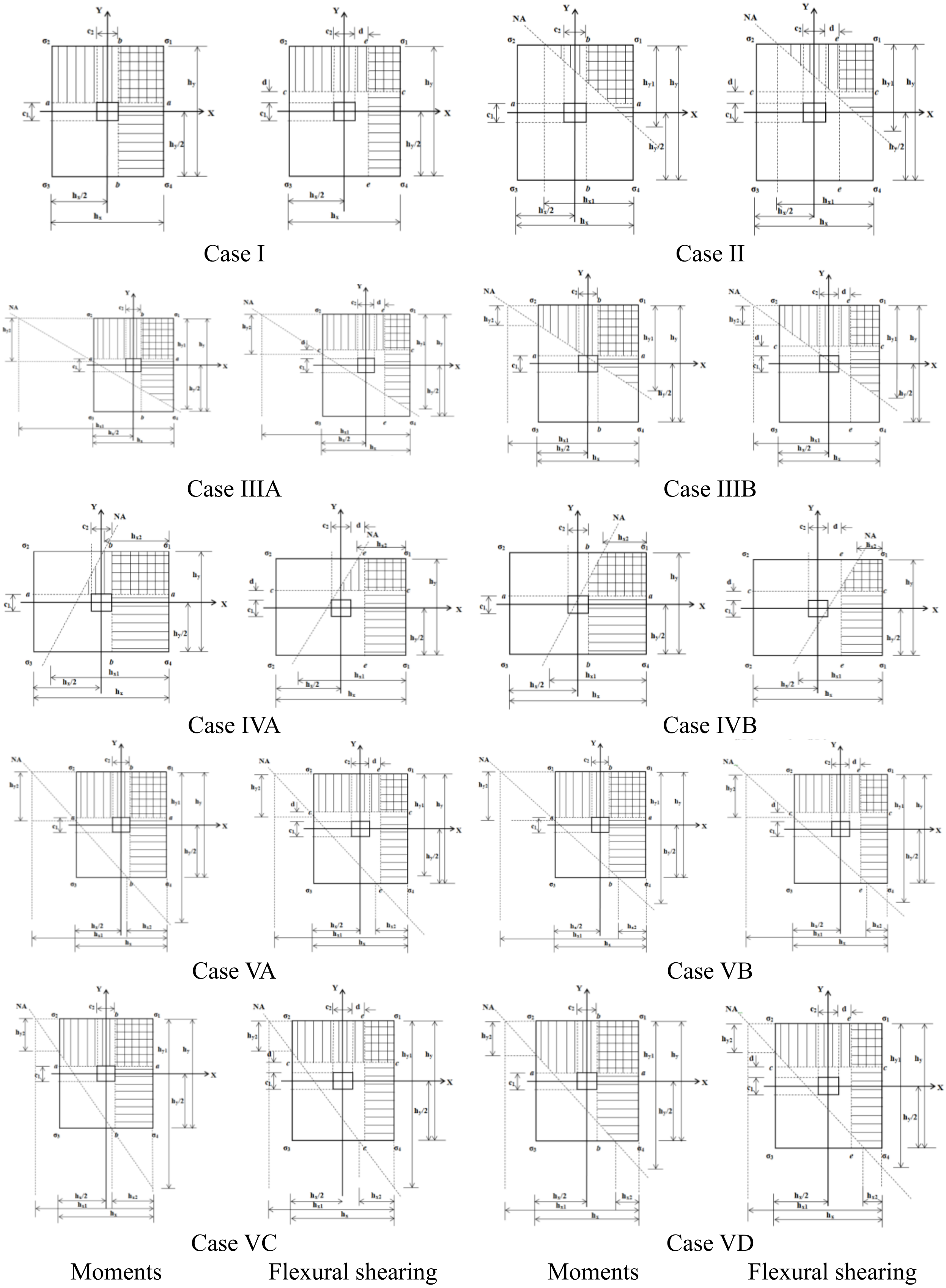


Figure 6. Moments and flexural shearing for biaxial bending
Source: Own elaboration

**Case I**
When $P$ is located inside the central nucleus
Equation (1) is substituted into Equations (5) to (8) and the integrals are developed to obtain the final equations.

**Case II**
When $P$ is located outside the central nucleus

$$V_{uc} = \int_{\frac{c_1}{2}+d}^{\frac{h_y}{2}} \int_{\frac{h_x}{2}+\frac{h_{x1}(h_y-2y)}{2h_{y1}}-h_{x1}}^{\frac{h_x}{2}} \sigma_z(x,y)dxdy \tag{29}$$

$$V_{ue} = \int_{\frac{c_2}{2}+d}^{\frac{h_x}{2}} \int_{\frac{h_y}{2}+\frac{h_{y1}(h_x-2x)}{2h_{x1}}-h_{y1}}^{\frac{h_y}{2}} \sigma_z(x,y)dydx \tag{30}$$

$$M_{ua} = \int_{\frac{c_1}{2}}^{\frac{h_y}{2}} \int_{\frac{h_x}{2}+\frac{h_{x1}(h_y-2y)}{2h_{y1}}-h_{x1}}^{\frac{h_x}{2}} \sigma_z(x,y)\left(y-\frac{c_1}{2}\right)dxdy \tag{31}$$

$$M_{ub} = \int_{\frac{c_2}{2}}^{\frac{h_x}{2}} \int_{\frac{h_y}{2}+\frac{h_{y1}(h_x-2x)}{2h_{x1}}-h_{y1}}^{\frac{h_y}{2}} \sigma_z(x,y)\left(x-\frac{c_2}{2}\right)dydx \tag{32}$$

**Case III**
When $P$ is located outside the central nucleus of two possible cases: Case IIIA when the neutral axis is located $h_y/2 - h_{y2} \leq c_1/2$ (moment) and $h_y/2 - h_{y2} \leq c_1/2 + d$ (flexural shearing); Case IIIB when the neutral axis is located $h_y/2 - h_{y2} \geq c_1/2$ (moment) and $h_y/2 - h_{y2} \geq c_1/2 + d$ (flexural shearing).

**Case IIIA**

$$V_{uc} = \int_{\frac{c_1}{2}+d}^{\frac{h_y}{2}} \int_{-\frac{h_x}{2}}^{\frac{h_x}{2}} \sigma_z(x,y)dxdy \tag{33}$$

$$V_{ue} = \int_{\frac{c_2}{2}+d}^{\frac{h_x}{2}} \int_{\frac{h_y}{2}+\frac{h_{y1}(h_x-2x)}{2h_{x1}}-h_{y1}}^{\frac{h_y}{2}} \sigma_z(x,y)dydx \tag{34}$$

$$M_{ua} = \int_{\frac{c_1}{2}}^{\frac{h_y}{2}} \int_{-\frac{h_x}{2}}^{\frac{h_x}{2}} \sigma_z(x,y)\left(y-\frac{c_1}{2}\right)dxdy \tag{35}$$

$$M_{ub} = \int_{\frac{c_2}{2}}^{\frac{h_x}{2}} \int_{\frac{h_y}{2}+\frac{h_{y1}(h_x-2x)}{2h_{x1}}-h_{y1}}^{\frac{h_y}{2}} \sigma_z(x,y)\left(x-\frac{c_2}{2}\right)dydx \tag{36}$$

**Case IIIB**

$$V_{uc}=\int_{\frac{c_1}{2}+d}^{\frac{h_y}{2}-h_{y2}}\int_{\frac{h_x}{2}+\frac{h_{x1}(h_y-2y)}{2h_{y1}}-h_{x1}}^{\frac{h_x}{2}}\sigma_z(x,y)dxdy+\int_{\frac{h_y}{2}-h_{y2}}^{\frac{h_y}{2}}\int_{-\frac{h_x}{2}}^{\frac{h_x}{2}}\sigma_z(x,y)dxdy \tag{37}$$

$$V_{ue}=\int_{\frac{c_2}{2}+d}^{\frac{h_x}{2}}\int_{\frac{h_y}{2}+\frac{h_{y1}(h_x-2x)}{2h_{x1}}-h_{y1}}^{\frac{h_y}{2}}\sigma_z(x,y)dydx \tag{38}$$

$$\begin{aligned}M_{ua}&=\int_{\frac{c_1}{2}}^{\frac{h_y}{2}-h_{y2}}\int_{\frac{h_x}{2}+\frac{h_{x1}(h_y-2y)}{2h_{y1}}-h_{x1}}^{\frac{h_x}{2}}\sigma_z(x,y)\left(y-\frac{c_1}{2}\right)dxdy\\&\quad+\int_{\frac{h_y}{2}-h_{y2}}^{\frac{h_y}{2}}\int_{-\frac{h_x}{2}}^{\frac{h_x}{2}}\sigma_z(x,y)\left(y-\frac{c_1}{2}\right)dxdy\end{aligned} \tag{39}$$

$$M_{ub}=\int_{\frac{c_2}{2}}^{\frac{h_x}{2}}\int_{\frac{h_y}{2}+\frac{h_{y1}(h_x-2x)}{2h_{x1}}-h_{y1}}^{\frac{h_y}{2}}\sigma_z(x,y)\left(x-\frac{c_2}{2}\right)dydx \tag{40}$$

where: $h_{y2} = h_{y1}(h_{x1} - h_x)/h_{x1}$.

**Case IV**

When $P$ is located outside the central nucleus of two possible cases: Case IVA when the neutral axis is located $h_x/2 - h_{x2} \leq c_2/2$ (moment) and $h_x/2 - h_{x2} \leq c_2/2 + d$ (flexural shearing); Case IIIB when the neutral axis is located $h_x/2 - h_{x2} \geq c_2/2$ (moment) and $h_x/2 - h_{x2} \geq c_2/2 + d$ (flexural shearing).

**Case IVA**

$$V_{uc}=\int_{\frac{c_1}{2}+d}^{\frac{h_y}{2}}\int_{\frac{h_x}{2}+\frac{h_{x1}(h_y-2y)}{2h_{y1}}-h_{x1}}^{\frac{h_x}{2}}\sigma_z(x,y)dxdy \tag{41}$$

$$V_{ue}=\int_{\frac{c_2}{2}+d}^{\frac{h_x}{2}}\int_{-\frac{h_y}{2}}^{\frac{h_y}{2}}\sigma_z(x,y)dydx \tag{42}$$

$$M_{ua}=\int_{\frac{c_1}{2}}^{\frac{h_y}{2}}\int_{\frac{h_x}{2}+\frac{h_{x1}(h_y-2y)}{2h_{y1}}-h_{x1}}^{\frac{h_x}{2}}\sigma_z(x,y)\left(y-\frac{c_1}{2}\right)dxdy \tag{43}$$

$$M_{ub}=\int_{\frac{c_2}{2}}^{\frac{h_x}{2}}\int_{-\frac{h_y}{2}}^{\frac{h_y}{2}}\sigma_z(x,y)\left(x-\frac{c_2}{2}\right)dydx \tag{44}$$

**Case IVB**

$$V_{uc} = \int_{\frac{c_1}{2}+d}^{\frac{h_y}{2}} \int_{\frac{h_x}{2}+\frac{h_{x1}(h_y-2y)}{2h_{y1}}-h_{x1}}^{\frac{h_x}{2}} \sigma_z(x,y)dxdy \tag{45}$$

$$V_{ue} = \int_{\frac{c_2}{2}+d}^{\frac{h_x}{2}-h_{x2}} \int_{\frac{h_y}{2}+\frac{h_{y1}(h_x-2x)}{2h_{x1}}-h_{y1}}^{\frac{h_y}{2}} \sigma_z(x,y)dydx + \int_{\frac{h_x}{2}-h_{x2}}^{\frac{h_x}{2}} \int_{-\frac{h_y}{2}}^{\frac{h_y}{2}} \sigma_z(x,y)dydx \tag{46}$$

$$M_{ua} = \int_{\frac{c_1}{2}}^{\frac{h_y}{2}} \int_{\frac{h_x}{2}+\frac{h_{x1}(h_y-2y)}{2h_{y1}}-h_{x1}}^{\frac{h_x}{2}} \sigma_z(x,y)\left(y-\frac{c_1}{2}\right)dxdy \tag{47}$$

$$\begin{aligned} M_{ub} = & \int_{\frac{c_2}{2}}^{\frac{h_x}{2}-h_{x2}} \int_{\frac{h_y}{2}+\frac{h_{y1}(h_x-2x)}{2h_{x1}}-h_{y1}}^{\frac{h_y}{2}} \sigma_z(x,y)\left(x-\frac{c_2}{2}\right)dydx \\ & + \int_{\frac{h_x}{2}-h_{x2}}^{\frac{h_x}{2}} \int_{-\frac{h_y}{2}}^{\frac{h_y}{2}} \sigma_z(x,y)\left(x-\frac{c_2}{2}\right)dydx \end{aligned} \tag{48}$$

where: $h_{x2} = h_{x1}(h_{y1} - h_y)/h_{y1}$.

**Case V**

When $P$ is located outside the central nucleus of four possible cases: Case VA when the neutral axis is localized $h_y/2 - h_{y2} \leq c_1/2 + d$ and $h_x/2 - h_{x2} \leq c_2/2 + d$ (flexural shearing) and $h_y/2 - h_{y2} \leq c_1/2$ and $h_x/2 - h_{x2} \leq c_2/2$ (moment); Case VB when the neutral axis is localized $h_y/2 - h_{y2} \leq c_1/2 + d$ and $h_x/2 - h_{x2} \geq c_2/2 + d$ (flexural shearing) and $h_y/2 - h_{y2} \leq c_1/2$ and $h_x/2 - h_{x2} \geq c_2/2$ (moment); Case VC when the neutral axis is localized $h_y/2 - h_{y2} \geq c_1/2 + d$ and $h_x/2 - h_{x2} \leq c_2/2 + d$ (flexural shearing) and $h_y/2 - h_{y2} \geq c_1/2$ and $h_x/2 - h_{x2} \leq c_2/2$ (moment); Case VD when the neutral axis is localized $h_y/2 - h_{y2} \geq c_1/2 + d$ and $h_x/2 - h_{x2} \geq c_2/2 + d$ (flexural shearing) and $h_y/2 - h_{y2} \geq c_1/2$ and $h_x/2 - h_{x2} \geq c_2/2$ (moment).

**Case VA**

$$V_{uc} = \int_{\frac{c_1}{2}+d}^{\frac{h_y}{2}} \int_{-\frac{h_x}{2}}^{\frac{h_x}{2}} \sigma_z(x,y)dxdy \tag{49}$$

$$V_{ue} = \int_{\frac{c_2}{2}+d}^{\frac{h_x}{2}} \int_{-\frac{h_y}{2}}^{\frac{h_y}{2}} \sigma_z(x,y)dydx \tag{50}$$

$$M_{ua} = \int_{\frac{c_1}{2}}^{\frac{h_y}{2}} \int_{-\frac{h_x}{2}}^{\frac{h_x}{2}} \sigma_z(x,y)\left(y-\frac{c_1}{2}\right)dxdy \tag{51}$$

$$M_{ub} = \int_{\frac{c_2}{2}}^{\frac{h_x}{2}} \int_{-\frac{h_y}{2}}^{\frac{h_y}{2}} \sigma_z(x,y)\left(x - \frac{c_2}{2}\right) dydx \tag{52}$$

**Case VB**

$$V_{uc} = \int_{\frac{c_1}{2}+d}^{\frac{h_y}{2}} \int_{-\frac{h_x}{2}}^{\frac{h_x}{2}} \sigma_z(x,y) dxdy \tag{53}$$

$$V_{ue} = \int_{\frac{c_2}{2}+d}^{\frac{h_x}{2}-h_{x2}} \int_{\frac{h_y}{2}+\frac{h_{y1}(h_x-2x)}{2h_{x1}}-h_{y1}}^{\frac{h_y}{2}} \sigma_z(x,y) dydx + \int_{\frac{h_x}{2}-h_{x2}}^{\frac{h_x}{2}} \int_{-\frac{h_y}{2}}^{\frac{h_y}{2}} \sigma_z(x,y) dydx \tag{54}$$

$$M_{ua} = \int_{\frac{c_1}{2}}^{\frac{h_y}{2}} \int_{-\frac{h_x}{2}}^{\frac{h_x}{2}} \sigma_z(x,y)\left(y - \frac{c_1}{2}\right) dxdy \tag{55}$$

$$\begin{aligned} M_{ub} = & \int_{\frac{c_2}{2}}^{\frac{h_x}{2}-h_{x2}} \int_{\frac{h_y}{2}+\frac{h_{y1}(h_x-2x)}{2h_{x1}}-h_{y1}}^{\frac{h_y}{2}} \sigma_z(x,y)\left(x - \frac{c_2}{2}\right) dydx \\ & + \int_{\frac{h_x}{2}-h_{x2}}^{\frac{h_x}{2}} \int_{-\frac{h_y}{2}}^{\frac{h_y}{2}} \sigma_z(x,y)\left(x - \frac{c_2}{2}\right) dydx \end{aligned} \tag{56}$$

**Case VC**

$$V_{uc} = \int_{\frac{c_1}{2}+d}^{\frac{h_y}{2}-h_{y2}} \int_{\frac{h_x}{2}+\frac{h_{x1}(h_y-2y)}{2h_{y1}}-h_{x1}}^{\frac{h_x}{2}} \sigma_z(x,y) dxdy + \int_{\frac{h_y}{2}-h_{y2}}^{\frac{h_y}{2}} \int_{-\frac{h_x}{2}}^{\frac{h_x}{2}} \sigma_z(x,y) dxdy \tag{57}$$

$$V_{ue} = \int_{\frac{c_2}{2}+d}^{\frac{h_x}{2}} \int_{-\frac{h_y}{2}}^{\frac{h_y}{2}} \sigma_z(x,y) dydx \tag{58}$$

$$\begin{aligned} M_{ua} = & \int_{\frac{c_1}{2}}^{\frac{h_y}{2}-h_{y2}} \int_{\frac{h_x}{2}+\frac{h_{x1}(h_y-2y)}{2h_{y1}}-h_{x1}}^{\frac{h_x}{2}} \sigma_z(x,y)\left(y - \frac{c_1}{2}\right) dxdy \\ & + \int_{\frac{h_y}{2}-h_{y2}}^{\frac{h_y}{2}} \int_{-\frac{h_x}{2}}^{\frac{h_x}{2}} \sigma_z(x,y)\left(y - \frac{c_1}{2}\right) dxdy \end{aligned} \tag{59}$$

$$M_{ub} = \int_{\frac{c_2}{2}}^{\frac{h_x}{2}} \int_{-\frac{h_y}{2}}^{\frac{h_y}{2}} \sigma_z(x,y)\left(x - \frac{c_2}{2}\right) dydx \tag{60}$$

**Case VD**

$$V_{uc}=\int_{\frac{c_1}{2}+d}^{\frac{h_y}{2}-h_{y2}}\int_{\frac{h_x}{2}+\frac{h_{x1}(h_y-2y)}{2h_{y1}}-h_{x1}}^{\frac{h_x}{2}}\sigma_z(x,y)dxdy+\int_{\frac{h_y}{2}-h_{y2}}^{\frac{h_y}{2}}\int_{-\frac{h_x}{2}}^{\frac{h_x}{2}}\sigma_z(x,y)dxdy \quad (61)$$

$$V_{ue}=\int_{\frac{c_2}{2}+d}^{\frac{h_x}{2}-h_{x2}}\int_{\frac{h_y}{2}+\frac{h_{y1}(h_x-2x)}{2h_{x1}}-h_{y1}}^{\frac{h_y}{2}}\sigma_z(x,y)dydx+\int_{\frac{h_x}{2}-h_{x2}}^{\frac{h_x}{2}}\int_{-\frac{h_y}{2}}^{\frac{h_y}{2}}\sigma_z(x,y)dydx \quad (62)$$

$$\begin{aligned}M_{ua}&=\int_{\frac{c_1}{2}}^{\frac{h_y}{2}-h_{y2}}\int_{\frac{h_x}{2}+\frac{h_{x1}(h_y-2y)}{2h_{y1}}-h_{x1}}^{\frac{h_x}{2}}\sigma_z(x,y)\left(y-\frac{c_1}{2}\right)dxdy\\&+\int_{\frac{h_y}{2}-h_{y2}}^{\frac{h_y}{2}}\int_{-\frac{h_x}{2}}^{\frac{h_x}{2}}\sigma_z(x,y)\left(y-\frac{c_1}{2}\right)dxdy\end{aligned} \quad (63)$$

$$\begin{aligned}M_{ub}&=\int_{\frac{c_2}{2}}^{\frac{h_x}{2}-h_{x2}}\int_{\frac{h_y}{2}+\frac{h_{y1}(h_x-2x)}{2h_{x1}}-h_{y1}}^{\frac{h_y}{2}}\sigma_z(x,y)\left(x-\frac{c_2}{2}\right)dydx\\&+\int_{\frac{h_x}{2}-h_{x2}}^{\frac{h_x}{2}}\int_{-\frac{h_y}{2}}^{\frac{h_y}{2}}\sigma_z(x,y)\left(x-\frac{c_2}{2}\right)dydx\end{aligned} \quad (64)$$

Note: Equation (4) is substituted into equations (29) to (64) and the integrals are developed to obtain the final equations.

### *2.2.2. Punching shearing*

Figure 7 shows the critical sections for punching shearing of six possible cases (Critical perimeter formed by points 5, 6, 7 and 8).

For case I, it is considered that the total surface of the footing works under compression. The pressure generated by the soil on the footing is obtained by equation (1) (biaxial bending).

For cases II, III, IV, V and VI consider that the total surface of the footing works partially under compression, i.e., part of the surface has zero pressure. The pressure generated by the soil on the footing is obtained by equation (4).

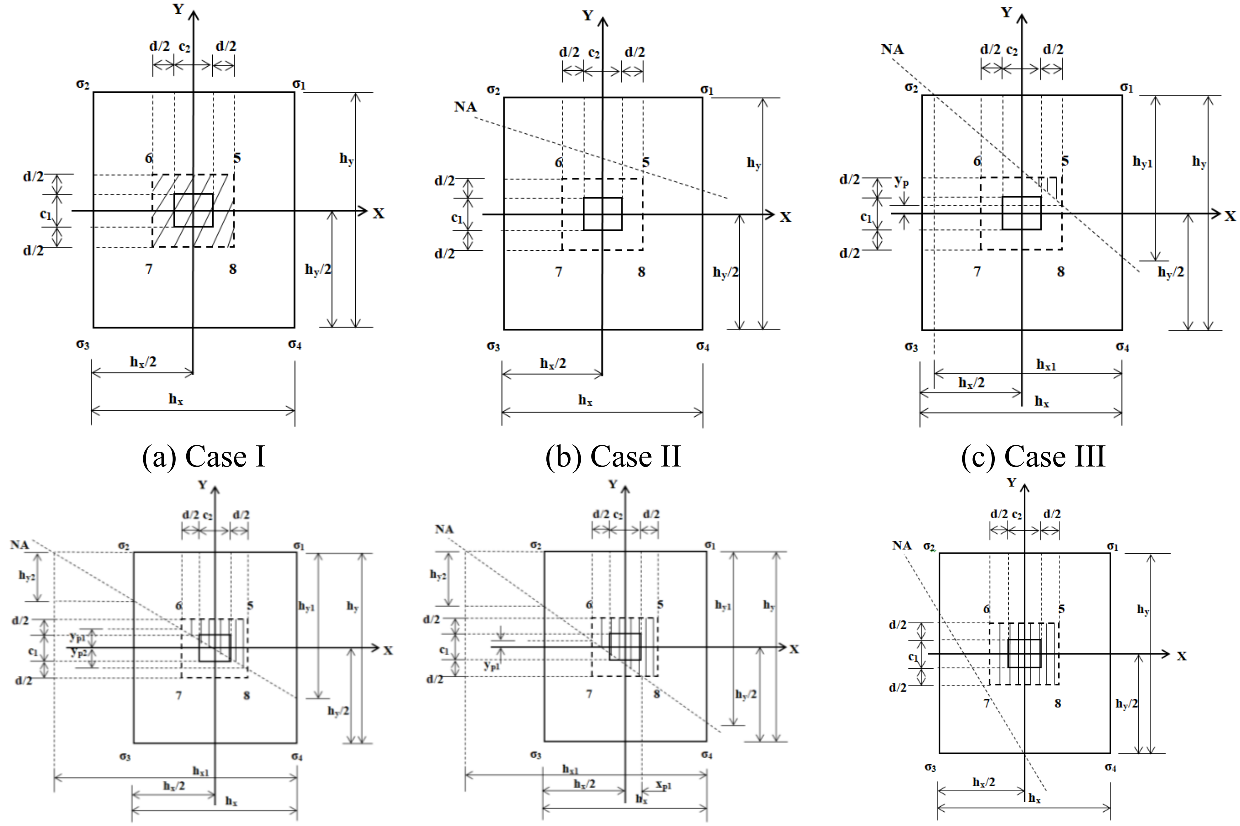


(a) Case I (b) Case II (c) Case III

(d) Case IV (e) Case V (f) Case VI

Figure 7. Punching shearing for biaxial bending
Source: Own elaboration

The general equation for the factorized punching shearing "$V_{up}$" is:

**Case I**
Equation (1) is substituted into equation (25) and the integral is developed to obtain the final equation.

**Case II**
The neutral axis does not reach the perimeter of the critical section; therefore, it is equation (26).

**Case III**

$$V_{up} = P_u - \int_{y_p}^{\frac{c_1}{2}+\frac{d}{2}} \int_{\frac{h_x}{2}-\frac{h_{x1}(2y-h_y)}{2h_{y1}}-h_{x1}}^{\frac{c_2}{2}+\frac{d}{2}} \sigma_z(x,y)\,dx\,dy \tag{65}$$

where: $y_p = h_y/2 - h_{y1}(c_2 + d - h_x)/2h_{x1} - h_{y1}$ (If the neutral axis crosses the critical perimeter on the side formed by points 5 and 8) and $y_p = -c_1/2 - d/2$ (If the neutral axis crosses the critical perimeter on the side formed by points 7 and 8).

**Case IV**

$$V_{up} = P_u - \int_{-\frac{c_2}{2}-\frac{d}{2}}^{\frac{c_2}{2}+\frac{d}{2}} \int_{\frac{h_y}{2}-\frac{h_{y1}(2x-h_x)}{2h_{x1}}-h_{y1}}^{y_{p1}} \sigma_z(x,y)dydx - \int_{-\frac{c_2}{2}-\frac{d}{2}}^{\frac{c_2}{2}+\frac{d}{2}} \int_{y_{p1}}^{\frac{c_1}{2}+\frac{d}{2}} \sigma_z(x,y)dydx \tag{66}$$

where: $y_{p1} = h_y/2 + h_{y1}(c_2 + d + h_x)/2h_{x1} - h_{y1}$.

**Case V**

$$V_{up} = P_u - \int_{-\frac{c_2}{2}-\frac{d}{2}}^{x_{p1}} \int_{\frac{h_y}{2}-\frac{h_{y1}(2x-h_x)}{2h_{x1}}-h_{y1}}^{y_{p1}} \sigma_z(x,y)dydx - \int_{-\frac{c_2}{2}-\frac{d}{2}}^{\frac{c_2}{2}+\frac{d}{2}} \int_{y_{p1}}^{\frac{c_1}{2}+\frac{d}{2}} \sigma_z(x,y)dydx - \int_{x_{p1}}^{\frac{c_2}{2}+\frac{d}{2}} \int_{-\frac{c_1}{2}-\frac{d}{2}}^{y_{p1}} \sigma_z(x,y)dydx \tag{67}$$

where: $x_{p1} = h_x/2 - h_{x1}(c_1 + d - h_y)/2h_{y1} - h_{x1}$ and $y_{p1} = h_y/2 + h_{y1}(c_2 + d + h_x)/2h_{x1} - h_{y1}$.

**Case VI**

$$V_{up} = P_u - \int_{-\frac{c_2}{2}-\frac{d}{2}}^{\frac{c_2}{2}+\frac{d}{2}} \int_{-\frac{c_1}{2}-\frac{d}{2}}^{\frac{c_1}{2}+\frac{d}{2}} \sigma_z(x,y)dydx \tag{68}$$

where: $x_{p1} = h_x/2 - h_{x1}(c_1 + d - h_y)/2h_{y1} - h_{x1}$ and $y_{p1} = h_y/2 + h_{y1}(c_2 + d + h_x)/2h_{x1} - h_{y1}$.
Note: Equation (4) is substituted into equations (65) to (68) and the integral are developed to obtain the final equations.

## 3. RESULTS

In this section the application of the new model is described, using the same examples to obtain the minimum area and the sides of a rectangular isolated footing proposed by Vela-Moreno et al. (2022).
Tables 1 and 2 present the four cases to obtain the complete design of the rectangular isolated footings subjected to uniaxial bending. Two cases when the axial load is located on the Y axis: Case I-Y, when the entire contact area works under compression; Case II-Y, when the contact area works partially in compression. Two cases when the axial load is located on the X axis: Case I-X, when the entire contact area works under compression; Case II-X, when the contact area works partially in compression.
Table 1 shows the results for $c_1$ and $c_2$ = 0.40 m, $P_u$ = 720 kN, $M_{ux}$ = 360, 720, 1440, 2160 kN-m, $M_{uy}$ = 0 kN-m and $\sigma_{umax}$ = 250 kN/m$^2$.
The procedure used is the following:
For the case I-Y: Substituting $P_u$, $M_{ux}$, $M_{uy}$ = 0, $h_x$, $h_y$ into equation (1), and subsequently substituting equation (1), $h_x$, $h_y$, $c_1$, $c_2$ and d into equations (5) to (8) and (25).
For the case II-Y: Substituting $\sigma_{umax}$, $h_y$, $h_{y1}$ into equation (2), and subsequently substituting equation (2), $h_x$, $h_y$, $c_1$, $c_2$ and d into equations (9) to (12) or (13) to (16), and (26) or (27) according to the case.
The value of *d* is fixed by the equations proposed by (ACI 318S-19).

Table 1. Complete design of the footing when the axial load is on the Y axis.
(Source: Own elaboration)

| Caso | $M_{ux}$ kN-m | $h_x$ m | $h_y$ m | d cm | $M_{ua}$ kN-m | $M_{ub}$ kN-m | $V_{uc}$ kN | $V_{ue}$ kN | $V_{up}$ kN | $A_{smy}$ $cm^2$ | $A_{sminy}$ $cm^2$ | $A_{spy}$ $cm^2$ | $A_{smx}$ $cm^2$ | $A_{sminx}$ $cm^2$ | $A_{spx}$ $cm^2$ |
|---|---|---|---|---|---|---|---|---|---|---|---|---|---|---|---|
| I-Y | 360 | 1.00 | 3.65 | 52 | 410.97 | 32.40 | 342.89 | * | 553.04 | 22.00 | 17.32 | 22.80 (8Ø3/4”) | 1.65 | 63.20 | 65.55 (23Ø3/4”) |
| II-Y | | 1.33 | 3.00 | 32 | 240.38 | 40.54 | 272.63 | 54.38 | 655.20 | 21.10 | 14.17 | 22.80 (8Ø3/4”) | 3.37 | 31.97 | 34.20 (12Ø3/4”) |
| I-Y | 720 | 1.00 | 6.00 | 67 | 794.45 | 32.40 | 420.46 | * | 582.61 | 33.32 | 22.31 | 34.20 (12Ø3/4”) | 1.28 | 133.87 | 136.89 (27Ø1”) |
| II-Y | | 1.00 | 4.67 | 52 | 468.41 | 22.50 | 322.24 | * | 631.92 | 25.28 | 17.32 | 25.65 (9Ø3/4”) | 1.15 | 80.87 | 81.12 (16Ø1”) |
| I-Y | 1440 | 2.00 | 12.00 | 42 | 1693.21 | 115.20 | 500.88 | 136.80 | 699.83 | 130.51 | 27.97 | 131.82 (26Ø1”) | 7.27 | 167.83 | 172.38 (34Ø1”) |
| II-Y | | 2.00 | 5.33 | 42 | 894.98 | 80.00 | 499.75 | 95.00 | 720.00 | 61.71 | 27.97 | 65.91 (13Ø1”) | 5.05 | 74.55 | 76.95 (27Ø3/4”) |
| I-Y | 2160 | 2.00 | 18.00 | 52 | 2592.81 | 115.20 | 510.05 | 100.80 | 703.07 | 161.36 | 34.63 | 162.24 (32Ø1”) | 5.87 | 311.69 | 314.34 (62Ø1”) |
| II-Y | | 2.00 | 7.33 | 37 | 1268.16 | 80.00 | 350.12 | 107.50 | 720.00 | 109.86 | 24.64 | 111.54 (22Ø1”) | 5.73 | 90.31 | 91.20 (32Ø3/4”) |

where: $A_{smy}$ and $A_{smx}$ are the steel areas generated by the moments in the *a* (Y direction) and *b* (X direction) axes, $A_{sminy}$ and $A_{sminx}$ are the minimum steel areas in both directions, $A_{spy}$ and $A_{spx}$ are the proposed steel areas in the Y and X directions (ACI 318S-19). * The axis is located outside the area of the footing.

Table 2 shows the results for $c_1$ and $c_2$ = 0.40 m, $P_u$ = 720 kN, $M_{ux}$ = 0 kN-m, $M_{uy}$ = 360, 720, 1440, 2160 kN-m and $\sigma_{umax}$ = 250 kN/m$^2$ (same procedure used in Table 1, but with the corresponding equations).

Table 2. Complete design of the footing when the axial load is on the X axis.
(Source: Own elaboration)

| Caso | $M_{uy}$ kN-m | $h_x$ m | $h_y$ m | d cm | $M_{ua}$ kN-m | $M_{ub}$ kN-m | $V_{uc}$ kN | $V_{ue}$ kN | $V_{up}$ kN | $A_{smy}$ $cm^2$ | $A_{sminy}$ $cm^2$ | $A_{spy}$ $cm^2$ | $A_{smx}$ $cm^2$ | $A_{sminx}$ $cm^2$ | $A_{spx}$ $cm^2$ |
|---|---|---|---|---|---|---|---|---|---|---|---|---|---|---|---|
| I-X | 360 | 3.65 | 1.00 | 52 | 32.40 | 410.97 | * | 342.89 | 553.04 | 1.65 | 63.20 | 65.55 (23Ø3/4”) | 22.00 | 17.32 | 22.80 (8Ø3/4”) |
| II-X | | 3.00 | 1.33 | 32 | 40.54 | 240.38 | 54.38 | 272.63 | 655.20 | 3.37 | 31.97 | 34.20 (12Ø3/4”) | 21.10 | 14.17 | 22.80 (8Ø3/4”) |
| I-X | 720 | 6.00 | 1.00 | 67 | 32.40 | 794.45 | * | 420.46 | 582.61 | 1.28 | 133.87 | 136.89 (27Ø1”) | 33.32 | 22.31 | 34.20 (12Ø3/4”) |
| II-X | | 4.67 | 1.00 | 52 | 22.50 | 468.41 | * | 322.24 | 631.92 | 1.15 | 80.87 | 81.12 (16Ø1”) | 25.28 | 17.32 | 25.65 (9Ø3/4”) |
| I-X | 1440 | 12.00 | 2.00 | 42 | 115.20 | 1693.21 | 136.80 | 500.88 | 699.83 | 7.27 | 167.83 | 172.38 (34Ø1”) | 130.51 | 27.97 | 131.82 (26Ø1”) |
| II-X | | 5.33 | 2.00 | 42 | 80.00 | 894.98 | 95.00 | 499.75 | 720.00 | 5.05 | 74.55 | 76.95 (27Ø3/4”) | 61.71 | 27.97 | 65.91 (13Ø1”) |
| I-X | 2160 | 18.00 | 2.00 | 52 | 115.20 | 2592.81 | 100.80 | 510.05 | 703.07 | 5.87 | 311.69 | 314.34 (62Ø1”) | 161.36 | 34.63 | 162.24 (32Ø1”) |
| II-X | | 7.33 | 2.00 | 37 | 80.00 | 1268.16 | 107.50 | 350.12 | 720.00 | 5.73 | 90.31 | 91.20 (32Ø3/4”) | 109.86 | 24.64 | 111.54 (22Ø1”) |

Tables 1 and 2 present the complete design of the rectangular isolated footings subjected to uniaxial bending.
Table 1 shows the following: The effective depth is governed by the flexural shearing in the *c* axis for the two cases ($M_{ux}$ = 360, 720, 1440 kN-m), and by the moment in the *a* axis for the two cases ($M_{ux}$ = 2160 kN-m). The smallest effective depth is presented in case II-Y for $M_{ux}$ = 360, 720, 2160 kN-m, and for $M_{ux}$ = 1440 kN-m the effective depth is the same in case I-Y and II-Y. The smallest proposed steel area appears in case II-Y for the two cases in both directions except at $M_{ux}$ = 360

kN-m which are the same in case I-Y and II-Y in Y direction.

Table 2 presents the following: The effective depth is governed by the flexural shearing in the *e* axis for the two cases ($M_{uy}$ = 360, 720, 1440 kN-m), and by the moment in the *b* axis for the two cases ($M_{uy}$ = 2160 kN-m). The smallest effective depth is presented in case II-X for $M_{uy}$ = 360, 720, 2160 kN-m, and for $M_{uy}$ = 1440 kN-m the effective depth is the same in case I-X and II-X. The smallest proposed steel area appears in case II-X for the two cases in both directions except at $M_{uy}$ = 360 kN-m which are the same in case I-X and II-X in X direction.

Tables 3 to 6 present the complete design of the rectangular isolated footings subjected to biaxial bending.

Tables 3 to 6 present the two cases to obtain the complete design of the isolated rectangular footings subjected to biaxial bending, a case when the entire contact area works under compression (Case I), and another case when the contact area works partially under compression (the smaller area of cases II, III, IV and V).

The procedure used for Tables 3 to 6 is as follows:

For case I: Substituting $P_u$, $M_{ux}$, $M_{uy}$, $h_x$, $h_y$ into equation (1), and later equation (1), $h_x$, $h_y$, $c_1$, $c_2$ and d is substituted into equations (5) to (8) and (25).

For cases II, III, IV and V: Substituting $\sigma_{umax}$, $h_x$, $h_{x1}$, $h_y$, $h_{y1}$ into equation (4), and subsequently substituting equation (4), $h_x$, $h_{x1}$, $h_y$, $h_{y1}$, $c_1$, $c_2$ and d into equations (29) to (32) (case II), into equations (33) to (36) (case IIIA), into equations (37) to (40) (case IIIB), into equations (41) to (44) (case IVA), into equations (45) to (48) (case IVB), into equations (49) to (52) (case VA), into equations (53) to (56) (case VB), into equations (57) to (60) (case VC), into equations (61) to (64) (case VD), and (26), (65) to (68) as the case may be.

Table 3 shows the results for $c_1$ and $c_2$ = 0.40 m, $P_u$ = 720 kN, $M_{ux}$ = 360, 720, 1440, 2160 kN-m, $M_{uy}$ = 360 kN-m and $\sigma_{umax}$ = 250 kN/m$^2$. The smallest area appears in the case V for $M_{ux}$ = 360 and 720 kN-m, and in the case II for $M_{ux}$ = 1440 and 2160 kN-m.

Table 3. Complete design of the footing for $M_{uy}$ = 360 kN-m.
(Source: Own elaboration)

| Caso | $M_{ux}$ kN-m | $h_x$ m | $h_y$ m | d cm | $M_{ua}$ kN-m | $M_{ub}$ kN-m | $V_{uc}$ kN | $V_{ue}$ kN | $V_{up}$ kN | $A_{smy}$ cm$^2$ | $A_{sminy}$ cm$^2$ | $A_{spy}$ cm$^2$ | $A_{smx}$ cm$^2$ | $A_{sminx}$ cm$^2$ | $A_{spx}$ cm$^2$ |
|---|---|---|---|---|---|---|---|---|---|---|---|---|---|---|---|
| I | 360 | 6.00 | 6.00 | 27 | 632.43 | 632.43 | 391.39 | 391.39 | 711.02 | 65.04 | 53.95 | 65.55 (23Ø3/4”) | 65.04 | 53.95 | 65.55 (23Ø3/4”) |
| V | | 2.72 | 2.72 | 22 | 229.25 | 229.25 | 305.04 | 305.04 | 698.58 | 29.25 | 19.93 | 31.35 (11Ø3/4”) | 29.25 | 19.93 | 31.35 (11Ø3/4”) |
| I | 720 | 6.00 | 12.00 | 27 | 1351.21 | 632.43 | 421.25 | 391.39 | 715.51 | 148.38 | 53.95 | 152.10 (30Ø1”) | 63.43 | 107.89 | 111.54 (22Ø1”) |
| V | | 2.22 | 4.45 | 27 | 472.00 | 196.31 | 367.54 | 298.13 | 709.58 | 51.44 | 19.93 | 55.77 (11Ø1”) | 19.61 | 40.01 | 42.75 (15Ø3/4”) |
| I | 1440 | 6.00 | 24.00 | 32 | 2790.60 | 632.43 | 434.23 | 384.90 | 717.41 | 278.09 | 63.94 | 278.85 (55Ø1”) | 52.71 | 255.74 | 258.57 (51Ø1”) |
| II | | 1.87 | 7.46 | 37 | 948.06 | 174.75 | 419.11 | 254.16 | 720.00 | 78.18 | 23.04 | 79.80 (16Ø1”) | 12.56 | 91.91 | 94.05 (33Ø3/4”) |
| I | 2160 | 6.00 | 36.00 | 42 | 4230.40 | 632.43 | 437.49 | 371.76 | 717.76 | 311.87 | 83.92 | 314.34 (62Ø1”) | 39.96 | 503.50 | 507.00 (100Ø1”) |
| II | | 1.71 | 10.24 | 42 | 1428.46 | 165.34 | 447.01 | 210.14 | 720.00 | 109.68 | 23.02 | 111.54 (22Ø1”) | 10.44 | 143.22 | 145.35 (51Ø3/4”) |

Table 3 shows the following: The effective depth is governed by the punching shearing for the two cases ($M_{ux}$ = 360, 720 kN-m), and by the moment in the *a* axis for the two cases ($M_{ux}$ = 1440, 2160 kN-m). The smallest effective depth occurs in case V for $M_{ux}$ = 360 kN-m, smallest effective depth occurs in case I for $M_{ux}$ = 1440 kN-m, and for $M_{ux}$ = 720, 2160 kN-m the effective depth is the same in both cases. The larger proposed steel area appears in case I for the two cases in both directions.

Table 4 shows the results for $c_1$ and $c_2$ = 0.40 m, $P_u$ = 720 kN, $M_{ux}$ = 360, 720, 1440, 2160 kN-m, $M_{uy}$ = 720 kN-m and $\sigma_{umax}$ = 250 kN/m$^2$. The smallest area appears in the case V for $M_{ux}$ = 360 kN-m, and in the case II for $M_{ux}$ = 720, 1440 and 2160 kN-m.

Table 4. Complete design of the footing for $M_{uy}$ = 720 kN-m.
(Source: Own elaboration)

| **Caso** | **$M_{ux}$ kN-m** | **$h_x$ m** | **$h_y$ m** | **d cm** | **$M_{ua}$ kN-m** | **$M_{ub}$ kN-m** | **$V_{uc}$ kN** | **$V_{ue}$ kN** | **$V_{up}$ kN** | **$A_{smy}$ cm$^2$** | **$A_{sminy}$ cm$^2$** | **$A_{spy}$ cm$^2$** | **$A_{smx}$ cm$^2$** | **$A_{sminx}$ cm$^2$** | **$A_{spx}$ cm$^2$** |
|---|---|---|---|---|---|---|---|---|---|---|---|---|---|---|---|
| I | 360 | 12.00 | 6.00 | 27 | 632.43 | 1351.21 | 391.39 | 421.25 | 715.51 | 63.43 | 107.89 | 111.54 (22Ø1”) | 148.38 | 53.95 | 152.10 (30Ø1”) |
| V | | 4.45 | 2.22 | 27 | 196.31 | 472.00 | 298.13 | 367.54 | 709.58 | 19.61 | 40.10 | 42.75 (15Ø3/4”) | 51.44 | 19.96 | 54.15 (19Ø3/4”) |
| I | 720 | 12.00 | 12.00 | 27 | 1351.21 | 1351.21 | 421.25 | 421.25 | 717.76 | 139.46 | 107.89 | 141.96 (28Ø1”) | 139.46 | 107.89 | 141.96 (28Ø1”) |
| II | | 3.73 | 3.73 | 27 | 430.31 | 430.31 | 392.78 | 392.78 | 720.00 | 44.47 | 33.54 | 45.63 (9Ø1”) | 44.47 | 33.54 | 45.63 (9Ø1”) |
| I | 1440 | 12.00 | 24.00 | 27 | 2790.60 | 1351.21 | 435.76 | 421.25 | 718.88 | 307.84 | 107.89 | 309.27 (61Ø1”) | 135.74 | 215.78 | 218.01 (51Ø1”) |
| II | | 3.22 | 6.45 | 27 | 913.51 | 408.86 | 458.25 | 423.74 | 720.00 | 104.20 | 28.95 | 106.47 (21Ø1”) | 41.21 | 57.99 | 59.85 (21Ø3/4”) |
| I | 2160 | 12.00 | 36.00 | 27 | 4230.40 | 1351.21 | 440.54 | 421.25 | 719.25 | 508.33 | 107.89 | 512.07 (101Ø1”) | 134.59 | 323.68 | 324.48 (64Ø1”) |
| II | | 3.00 | 9.00 | 32 | 1404.83 | 403.75 | 480.92 | 433.67 | 720.00 | 140.24 | 31.97 | 141.96 (28Ø1”) | 33.85 | 95.90 | 96.90 (34Ø3/4”) |

Table 5 shows the results for $c_1$ and $c_2$ = 0.40 m, $P_u$ = 720 kN, $M_{ux}$ = 360, 720, 1440, 2160 kN-m, $M_{uy}$ = 1440 kN-m and $\sigma_{umax}$ = 250 kN/m$^2$. The smallest area appears in the case II for $M_{ux}$ = 360, 720, 1440 and 2160 kN-m.

Table 5. Complete design of the footing for $M_{uy}$ = 1440 kN-m.
(Source: Own elaboration)

| **Caso** | **$M_{ux}$ kN-m** | **$h_x$ m** | **$h_y$ m** | **d cm** | **$M_{ua}$ kN-m** | **$M_{ub}$ kN-m** | **$V_{uc}$ kN** | **$V_{ue}$ kN** | **$V_{up}$ kN** | **$A_{smy}$ cm$^2$** | **$A_{sminy}$ cm$^2$** | **$A_{spy}$ cm$^2$** | **$A_{smx}$ cm$^2$** | **$A_{sminx}$ cm$^2$** | **$A_{spx}$ cm$^2$** |
|---|---|---|---|---|---|---|---|---|---|---|---|---|---|---|---|
| I | 360 | 24.00 | 6.00 | 32 | 632.43 | 2790.60 | 384.90 | 434.23 | 717.41 | 52.71 | 255.74 | 258.57 (51Ø1”) | 278.09 | 63.94 | 278.85 (55Ø1”) |
| II | | 7.46 | 1.87 | 37 | 174.75 | 948.06 | 254.16 | 419.11 | 720.00 | 12.56 | 91.91 | 94.05 (33Ø3/4”) | 78.18 | 23.04 | 79.80 (16Ø1”) |
| I | 720 | 24.00 | 12.00 | 27 | 1351.21 | 2790.60 | 421.25 | 435.76 | 718.88 | 135.74 | 215.78 | 218.01 (51Ø1”) | 307.84 | 107.89 | 309.27 (61Ø1”) |
| II | | 6.45 | 3.22 | 27 | 408.86 | 913.51 | 423.74 | 458.25 | 720.00 | 41.21 | 57.99 | 59.85 (21Ø3/4”) | 104.20 | 28.95 | 106.47 (21Ø1”) |
| I | 1440 | 24.00 | 24.00 | 27 | 2790.60 | 2790.60 | 435.76 | 435.76 | 719.44 | 288.54 | 215.78 | 288.99 (57Ø1”) | 288.54 | 215.78 | 288.99 (57Ø1”) |
| II | | 5.73 | 5.73 | 27 | 899.07 | 899.07 | 484.27 | 484.27 | 720.00 | 94.95 | 51.52 | 96.33 (19Ø1”) | 94.95 | 51.52 | 96.33 (19Ø1”) |
| I | 2160 | 24.00 | 36.00 | 27 | 4230.40 | 2790.60 | 440.54 | 435.76 | 719.63 | 451.51 | 215.78 | 456.30 (90Ø1”) | 283.13 | 323.68 | 324.48 (64Ø1”) |
| II | | 5.41 | 8.12 | 32 | 1399.94 | 898.75 | 498.17 | 495.32 | 720.00 | 157.03 | 48.64 | 157.17 (31Ø1”) | 92.67 | 73.01 | 94.05 (33Ø3/4”) |

Table 4 shows the following: The effective depth is governed by the punching shearing for the two cases ($M_{ux}$ = 360, 720, 1440 kN-m), and by the moment in the *a* axis for the two cases ($M_{ux}$ = 2160 kN-m). The smallest effective depth occurs in case I for $M_{ux}$ = 2160 kN-m, and for $M_{ux}$ = 360, 720, 1440 kN-m the effective depth is the same in both cases. The larger proposed steel area appears in case I for the two cases in both directions.
Table 5 shows the following: The effective depth is governed by the punching shearing for the two cases ($M_{ux}$ = 720, 1440, 2160 kN-m), and by the moment in the *a* axis for the two cases ($M_{ux}$ = 360 kN-m). The smallest effective depth occurs in case I for $M_{ux}$ = 360 kN-m, and for $M_{ux}$ = 720, 1440,

2160 kN-m the effective depth is the same in both cases. The larger proposed steel area appears in case I for the two cases in both directions.

Table 6 shows the results for $c_1$ and $c_2$ = 0.40 m, $P_u$ = 720 kN, $M_{ux}$ = 360, 720, 1440, 2160 kN-m, $M_{uy}$ = 2160 kN-m and $\sigma_{umax}$ = 250 kN/m$^2$. The smallest area appears in the case II for $M_{ux}$ = 360, 720, 1440 and 2160 kN-m.

Table 6. Complete design of the footing for $M_{uy}$ = 2160 kN-m.
(Source: Own elaboration)

| **Caso** | **$M_{ux}$ kN-m** | **$h_x$ m** | **$h_y$ m** | **d cm** | **$M_{ua}$ kN-m** | **$M_{ub}$ kN-m** | **$V_{uc}$ kN** | **$V_{ue}$ kN** | **$V_{up}$ kN** | **$A_{smy}$ cm$^2$** | **$A_{sminy}$ cm$^2$** | **$A_{spy}$ cm$^2$** | **$A_{smx}$ cm$^2$** | **$A_{sminx}$ cm$^2$** | **$A_{spx}$ cm$^2$** |
|---|---|---|---|---|---|---|---|---|---|---|---|---|---|---|---|
| I | 360 | 36.00 | 6.00 | 42 | 632.43 | 4230.40 | 371.76 | 437.49 | 717.76 | 39.96 | 503.50 | 507.00 (100Ø1”) | 311.87 | 83.92 | 314.34 (62Ø1”) |
| II | | 10.24 | 1.71 | 42 | 165.34 | 1428.46 | 210.14 | 447.01 | 720.00 | 10.44 | 143.22 | 145.35 (51Ø3/4”) | 109.68 | 23.92 | 111.54 (22Ø1”) |
| I | 720 | 36.00 | 12.00 | 27 | 1351.21 | 4230.40 | 421.25 | 440.54 | 719.63 | 134.59 | 323.68 | 324.48 (64Ø1”) | 307.84 | 107.89 | 309.27 (61Ø1”) |
| II | | 9.00 | 3.00 | 32 | 403.75 | 1404.83 | 433.67 | 480.92 | 720.00 | 33.85 | 95.90 | 96.90 (34Ø3/4”) | 140.24 | 31.97 | 141.96 (28Ø1”) |
| I | 1440 | 36.00 | 24.00 | 27 | 2790.60 | 4230.40 | 435.76 | 440.54 | 719.44 | 283.13 | 323.68 | 324.48 (64Ø1”) | 451.51 | 215.78 | 456.30 (90Ø1”) |
| II | | 8.12 | 5.41 | 27 | 898.75 | 1399.94 | 495.32 | 498.17 | 720.00 | 92.67 | 73.01 | 94.05 (33Ø3/4”) | 157.03 | 48.64 | 157.17 (31Ø1”) |
| I | 2160 | 36.00 | 36.00 | 27 | 4230.40 | 4230.40 | 440.54 | 440.54 | 719.75 | 437.69 | 323.68 | 441.09 (87Ø1”) | 437.69 | 323.68 | 441.09 (87Ø1”) |
| II | | 7.73 | 7.73 | 32 | 1396.69 | 1396.69 | 498.81 | 498.81 | 720.00 | 149.44 | 69.50 | 152.10 (30Ø1”) | 149.44 | 69.50 | 152.10 (30Ø1”) |

Table 6 shows the following: The effective depth is governed by the punching shearing for the two cases ($M_{ux}$ = 1440, 2160 kN-m), and by the moment in the *a* axis for the two cases ($M_{ux}$ = 360, 720 kN-m). The smallest effective depth occurs in case I for $M_{ux}$ = 720 kN-m, and for $M_{ux}$ = 360, 1440, 2160 kN-m the effective depth is the same in both cases. The larger proposed steel area appears in case I for the two cases in both directions.

Figure 8 shows the comparison for uniaxial bending (Axial load on the Y axis) of the current model (Case I-Y) and new model (Case II-Y) in terms of volume of concrete and steel of the considered examples.

Figure 8 shows the following: The new model presents smaller volumes of concrete and steel in all cases than the current model. The smallest difference in volumes of concrete and steel occurs at $M_{ux}$ = 360 kN-m of 1.37 times for concrete and 1.31 times for steel. The biggest difference in volumes of concrete and steel occurs at $M_{ux}$ = 2160 kN-m of 3.27 times for concrete and 3.55 times for steel.

Figure 9 shows the comparison for uniaxial bending (Axial load on the X axis) of the current model (Case I-X) and new model (Case II-X) in terms of volume of concrete and steel of the considered examples.

Figure 9 presents the following: The new model presents smaller volumes of concrete and steel in all cases than the current model. The smallest difference in volumes of concrete and steel occurs at $M_{uy}$ = 360 kN-m of 1.37 times for concrete and 1.31 times for steel. The biggest difference in volumes of concrete and steel occurs at $M_{uy}$ = 2160 kN-m of 3.27 times for concrete and 3.55 times for steel.

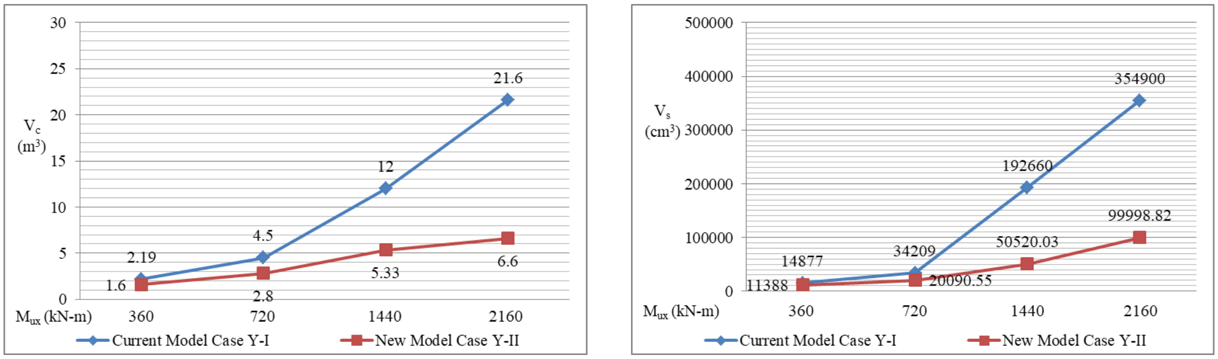


(a) Concrete (b) Steel

Figure 8. Comparison for uniaxial bending ($M_{uy} = 0$)

Source: Own elaboration

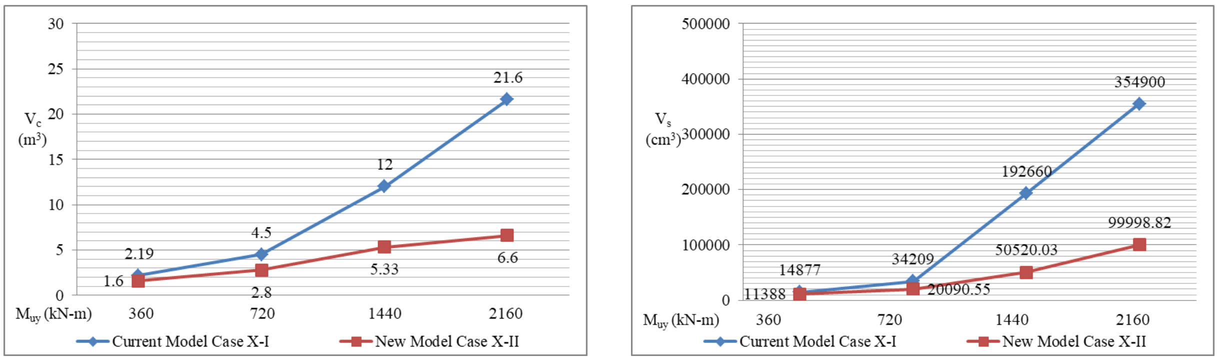


(a) Concrete (b) Steel

Figure 9. Comparison for uniaxial bending ($M_{ux} = 0$)

Source: Own elaboration

Figure 10 shows the comparison for biaxial bending of the current model (Case I) and new model (Case II or V) in terms of volume of concrete and steel of the considered examples.

Figure 10 shows the following:

The new model presents smaller volumes of concrete and steel in all cases than the current model.
The smallest differences occur at $M_{ux}$ = 360 kN-m for all cases in the volumes of concrete and steel of 5.68 times for concrete and 4.61 times for steel ($M_{uy}$ = 360 kN-m), 7.28 times for concrete and 7.43 times for steel ($M_{uy}$ = 720 kN-m), 9.17 times for concrete and 10.69 times for steel ($M_{uy}$ = 1440 kN-m), 12.33 times for concrete and 10.32 times for steel ($M_{uy}$ = 2160 kN-m).
The largest differences occur at $M_{ux}$ = 2160 kN-m for all cases in the volumes of concrete and steel of 12.33 times for concrete and 10.32 times for steel ($M_{uy}$ = 360 kN-m), 14.00 times for concrete and 14.24 times for steel ($M_{uy}$ = 720 kN-m), 19.66 times for concrete and 13.57 times for steel ($M_{uy}$ = 1440 kN-m), 21.69 times for concrete and 13.51 times for steel ($M_{uy}$ = 2160 kN-m).

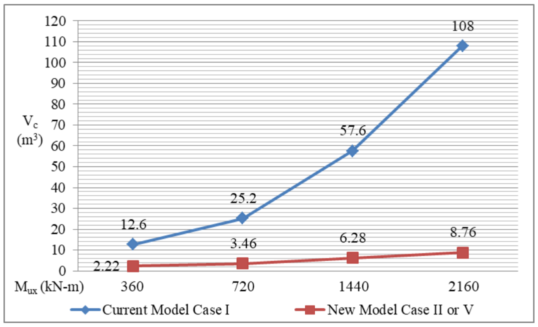


(a) $M_{uy}$ = 360 kN-m

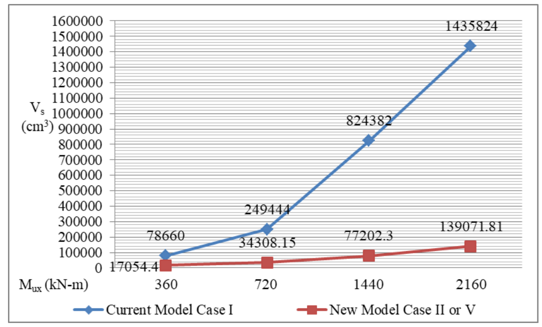


(b) $M_{uy}$ = 360 kN-m

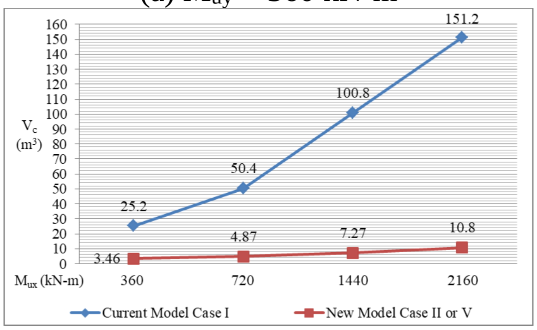


(c) $M_{uy}$ = 720 kN-m

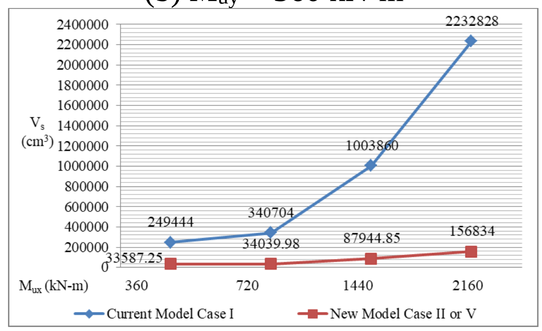


(d) $M_{uy}$ = 720 kN-m

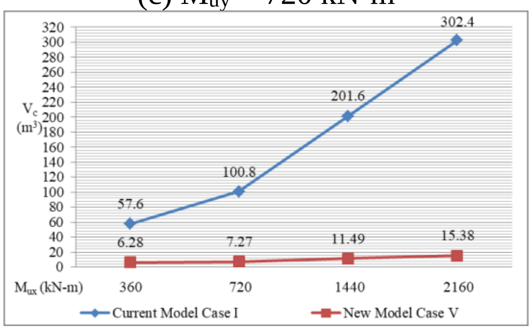


(e) $M_{uy}$ = 1440 kN-m

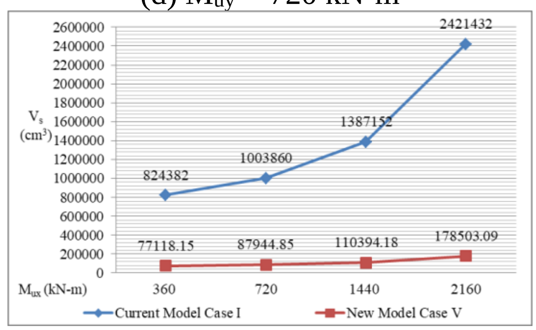


(f) $M_{uy}$ = 1440 kN-m

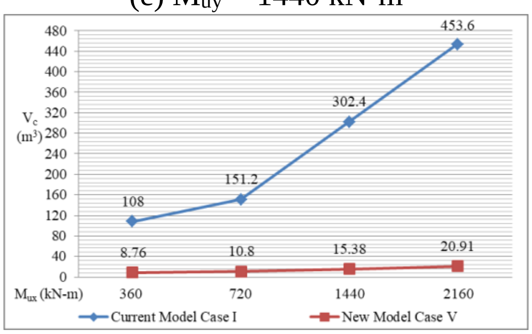


(g) $M_{uy}$ = 2160 kN-m

Concrete

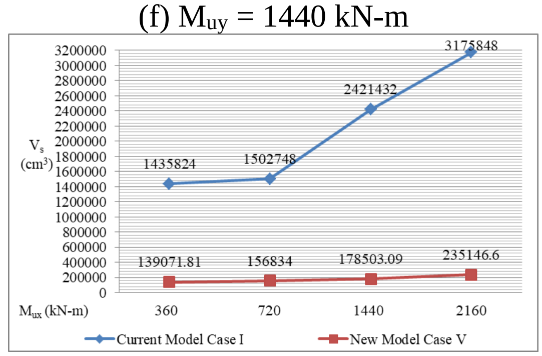


(h) $M_{uy}$ = 2160 kN-m

Steel

Figure 10. Comparison for biaxial bending

Source: Own elaboration

## 4. CONCLUSIONS

This work presents a new complete design mathematical model to obtain the thicknesses and areas of transverse and longitudinal steel for rectangular isolated footings subjected to uniaxial and biaxial bending supported on elastic soils, which considers the total surface working partially under compression and it is assumed that the distribution of pressures on the ground is linear.

The main contributions in this work are:
The main contributions of this work for these examples are:
1.- This work shows a significant reduction in the volumes of concrete and steel than the current model, if the contact surface with the ground working partially under compression.
2.- This work shows a significant reduction in the volume of excavation than the current model, because the new model occupies less volume.
3.- The thickness for both models are governed by moments and flexural shearing for uniaxial bending, and by moments and punching shearing for biaxial bending.
4.- The new model can be used for any building code, simply taking into account the moments, the flexural shearing and the punching shearing that resist to define the effective depth, and the equations to determine the reinforcing steel areas proposed by each building code.
5.- The new model can be used when the load $P_u$ is located outside the central nucleus ($e_x/h_x + e_y/h_y > 1/6$), and the current model is used when load $P_u$ is located inside the central nucleus ($e_x/h_x + e_y/h_y \leq 1/6$), where $e_x = M_y/P$ and $e_y = M_x/P$.
This works shows an effective and robust solution applied to obtain the complete design for rectangular isolated footings subjected to uniaxial and biaxial bending supported on elastic soils working partially under compression, and the variation of the pressure diagram is linear.
The suggestions for the next research:
1.- Complete design for combined footing (rectangular, trapezoidal, strap, corner and shaped-T) subjected to uniaxial and biaxial bending supported on elastic soils working partially under compression.
2.- Footings supported on totally cohesive soils (clay soils) and/or totally granular soils (sandy soils), the pressure diagram is different, because the pressure diagram is not linear as it is presented in this work.

## 5. REFERENCES

ACI 318S-19 (2019), "*Building Code Requirements for Structural Concrete and Commentary*, Committee 318", New York, USA.

Aguilera-Mancilla, G., Luévanos-Rojas, A., López-Chavarría, S. and Medina-Elizondo, M. (2019), *Modeling for the strap combined footings Part I: Optimal dimensioning*. Steel and Composite Structures. 30(2):97-108. https://doi.org/10.12989/scs.2019.30.2.097

Al-Gahtani, H.J. and Adekunle, S.K. (2019), *A boundary-type approach for the computation of vertical stresses in soil due to arbitrarily shaped foundations*. World Journal of Engineering. 16(3): 419-426. https://doi.org/10.1108/WJE-02-2018-0051

Algin, H.M. (2000), *Stresses from linearly distributed pressures over rectangular areas*. International Journal for Numerical and Analytical Methods in Geomechanics. 24(8):681-692. https://doi.org/10.1002/1096-9853(200007)24:8<681::AID-NAG89>3.0.CO;2-X

Algin, H.M. (2007), *Practical formula for dimensioning a rectangular footing*. Engineering Structures. 29(6):1128-1134. https://doi.org/10.1016/j.engstruct.2006.08.009

Aydogdu, I. (2016), *New Iterative method to Calculate Base Stress of Footings under Biaxial Bending*. Journal of Engineering and Applied Sciences. 8(4):40-48. https://doi.org/10.24107/ijeas.281460

Bezmalinovic Colleoni, A.S. (2016), *Fórmulas analíticas para la presión de contacto lineal en fundaciones rectangulares altamente excéntricas*. IX Chilean Congress on Geotechnical Engineering, Chilean Geotechnical Society, Universidad Austral de Chile.

Dagdeviren, U. (2016), *Shear stresses below the rectangular foundations subjected to biaxial bending*, Geomechanics Engineering. 10(2):189-205. https://doi.org/10.12989/gae.2016.10.2.189

Filho, W.L., Carvalho, R.CH., Christoforo, A.L. and Lahr, F.A.R. (2017), *Dimensioning of Isolated Footing Submitted to the under Biaxial Bending Considering the Low Concrete Consumption*. International Journal of Materials Engineering. 7(1):1-11. http://article.sapub.org/10.5923.j.ijme.20170701.01.html

Galvis, F.A. and Smith-Pardo, J.P. (2020), *Axial load biaxial moment interaction (PMM) diagrams for shallow foundations: Design aids, experimental verification, and examples*. Engineering Structures. 213:110582. https://doi.org/10.1016/j.engstruct.2020.110582

Girgin, K. (2017), *Simplified formulations for the determination of rotational spring constants in rigid spread footings resting on tensionless soil*. Journal Civil Engineering and Management. 23(4):464-474. https://doi.org/10.3846/13923730.2016.1210218

Gör, M. (2022), *Analyzing the bearing capacity of shallow foundations on two-layered soil using two novel cosmology-based optimization techniques*. Smart Structures and Systems. 29(3):513-522. https://doi.org/10.12989/sss.2022.29.3.513

Irles-Más, R. and Irles-Más, F. (1992), *Alternativa analítica a la determinación de tensiones bajo zapatas rectangulares con flexión biaxial y despegue parcial*. Informes de la Construcción. 44(419):77-89. https://dialnet.unirioja.es/servlet/articulo?codigo=2768804

Jahanandish, M., Veiskarami, M. and Ghahramani, A. (2012), *Effect of Foundation Size and Roughness on the Bearing Capacity Factor, Nγ, by Stress Level-Based ZEL Method*. Arabian Journal for Science and Engineering. 37(7):1817-1831. https://doi.org/10.1007/s13369-012-0293-3

Kaur, A. and Kumar, A. (2016), *Behavior of eccentrically inclined loaded footing resting on fiber reinforced soil*. Geomechanics Engineering. 10(2):155-174. https://doi.org/10.12989/gae.2016.10.2.155

Khajehzadeh, M., Taha M.R. and Eslami, M. (2014), *Multi-objective Optimization of foundation using global-local gravitational search algorithm*. Structural Engineering and Mechanics. 50(3): 257-273. https://doi.org/10.12989/sem.2014.50.3.257

Kim-Sánchez, D.S., Luévanos-Rojas, A., Barquero-Cabrero, J.D., López-Chavarría, S., Medina-Elizondo, M. and Luévanos-Soto, I. (2022). *A New Model for the Complete Design of Circular Isolated Footings Considering that the Contact Surface Works Partially under Compression*. International Journal of Innovative Computing, Information and Control. 18(6):1769-1784. http://www.ijicic.org/ijicic-180607.pdf

Lee, J., Jeong, S. and Lee, J.K. (2015), *3D analytical method for mat foundations considering coupled soil springs*. Geomechanics Engineering. 8(6):845-850. https://doi.org/10.12989/gae.2015.8.6.845

Lezgy-Nazargah, M., Mamazizi, A. and Khosravi, H. (2022), *Analysis of shallow footings rested on tensionless foundations using a mixed finite element model*. Structural Engineering and Mechanics. 81(3):379-394. https://doi.org/10.12989/sem.2022.81.3.379

López-Chavarría, S., Luévanos-Rojas, A. and Medina-Elizondo, M. (2017a), *A mathematical model for dimensioning of square isolated footings using optimization techniques: general case*. International Journal of Innovative Computing, Information and Control. 13(1):67-74. http://www.ijicic.org/ijicic-130105.pdf

López-Chavarría, S., Luévanos-Rojas, A. and Medina-Elizondo, M. (2017b), *Optimal dimensioning for the corner combined footings*. Advances in Computational Design. 2(2):169-183. https://doi.org/10.12989/acd.2017.2.2.169

López-Chavarría, S., Luévanos-Rojas, A. and Medina-Elizondo, M. (2017c), *A new mathematical model for design of square isolated footings for general case*. International Journal of Innovative Computing, Information and Control. 13(4):1149-1168. http://www.ijicic.org/ijicic-130406.pdf

López-Chavarría, S., Luévanos-Rojas, A., Medina-Elizondo, M., Sandoval-Rivas, R. and Velázquez-Santillán, F. (2019), *Optimal design for the reinforced concrete circular isolated footings*. Advances in Computational Design. 4(3):273-294. https://doi.org/10.12989/acd.2019.4.3.273

Luévanos-Rojas, A. (2012a), *A Mathematical Model for Dimensioning of Footings Square*. International Review of Civil Engineering. 3(4):346-350.

Luévanos-Rojas, A. (2012b), *A Mathematical Model for the Dimensioning of Circular Footings*. Far East Journal of Mathematical Sciences. 71(2): 357-367.

Luévanos-Rojas, A. (2013), *A Mathematical Model for Dimensioning of Footings Rectangular*. ICIC Express Letters Part B: Applications**.** 4(2):269-274.

Luévanos-Rojas, A., Faudoa-Herrera, J.G., Andrade-Vallejo, R.A. and Cano-Alvarez, M.A. (2013), *Design of Isolated Footings of Rectangular Form Using a New Model*. International Journal of Innovative Computing, Information and Control. 9(10):4001-4022. http://www.ijicic.org/ijicic-12-10031.pdf

Luévanos-Rojas, A. (2014a), A Comparative Study for Dimensioning of Footings with Respect to the Contact Surface on Soil. International Journal of Innovative Computing, Information and Control. 10(4):1313-1326. http://www.ijicic.org/ijicic-13-08003.pdf

Luévanos-Rojas, A. (2014b), *Design of isolated footings of circular form using a new model*. Structural Engineering and Mechanics. 52(4):767-786. http://dx.doi.org/10.12989/sem.2014.52.4.767

Luévanos-Rojas, A. (2014c), *Design of boundary combined footings of rectangular shape using a new model*. DYNA Colombia. 81(188):199-208. https://doi.org/10.15446/dyna.v81n188.41800

Luévanos-Rojas, A. (2015a), *A New Approach for Dimensioning of Rectangular Footings Using Optimization Techniques*. ICIC Express Letters Part B: Applications**.** 6(11):3141-3146.

Luévanos-Rojas, A. (2015b), *A New Mathematical Model for Dimensioning of the Boundary Trapezoidal Combined Footings*. International Journal of Innovative Computing, Information and Control. 11(4):1269-1279. http://www.ijicic.org/ijicic-110411.pdf

Luévanos-Rojas, A. (2015c), *A new model for the design of rectangular combined boundary footings with two restricted opposite sides*. Revista ALCONPAT. 6(2):172-187. http://dx.doi.org/10.21041/ra.v6i2.137

Luévanos-Rojas, A. (2015d), *Design of boundary combined footings of trapezoidal form using a new model*. Structural Engineering and Mechanics. 56(5):745-765. https://doi.org/10.12989/sem.2015.56.5.745

Luévanos-Rojas, A. (2016a), *A Mathematical Model for the Dimensioning of Combined Footings of Rectangular Shape*. Revista Técnica de la Facultad de Ingeniería Universidad del Zulia. 39(1):3-9. https://produccioncientificaluz.org/index.php/tecnica/article/view/21090/20946

Luévanos-Rojas, A. (2016b), *Un nuevo modelo para diseño de zapatas combinadas rectangulares de lindero con dos lados opuestos restringidos*. Revista ACONPAT. 6(2):173-189. http://dx.doi.org/10.21041/ra.v6i2.137

Luévanos-Rojas, A., López-Chavarría, S. and Medina-Elizondo, M. (2017), *Optimal design for rectangular isolated footings using the real soil pressure*. Ingeniería e Investigación. 37(2):25-33. http://dx.doi.org/10.15446/ing.investig.v37n2.61447

Luévanos-Rojas, A., López-Chavarría, S. and Medina-Elizondo, M. (2018a), *A new model for T-shaped combined footings Part I: Optimal dimensioning*. Geomechanics Engineering. 14(1):51-60. https://doi.org/10.12989/gae.2018.14.1.051

Luévanos-Rojas, A., López-Chavarría, S. and Medina-Elizondo, M. (2018b), *A new model for T-shaped combined footings Part II: Mathematical model for design*. Geomechanics Engineering. 14(1):61-69. https://doi.org/10.12989/gae.2018.14.1.061

Luévanos Rojas, A., López Chavarría, S., Medina Elizondo, M., Sandoval Rivas, R., Farías Montemayor, O. M. (2020), *Un modelo analítico para el diseño de zapatas combinadas de esquina*. Revista ALCONPAT. 10(3):317-335. https://doi.org/10.21041/ra.v10i3.432

Özmen, G. (2011), *Determination of Base Stresses in Rectangular Footings under Biaxial Bending*. Teknik Dergi Digest. 22(4):1519-1535. http://www.imo.org.tr/resimler/dosya_ekler/7b559795bd3f63b_ek.pdf?dergi=472

Rawat, S., Mittal, R.K. and Muthukumar, G. (2020), *Isolated Rectangular Footings under Biaxial Bending: A Critical Appraisal and Simplified Analysis Methodology*. Practice Periodical on Structural Design and Construction. 25(3):04020011. https://doi.org/10.1061/(ASCE)SC.1943-5576.0000471

Rodriguez-Gutierrez, J.A. and Aristizabal-Ochoa, J.D. (2013a), *Rigid Spread Footings Resting on Soil Subjected to Axial Load and Biaxial Bending. I: Simplified Analytical Method*. International Journal of Geomechanics. 13(2):109-119. https://doi.org/10.1061/(ASCE)GM.1943-5622.0000218

Rodriguez-Gutierrez, J.A. and Aristizabal-Ochoa, J.D. (2013b), *Rigid Spread Footings Resting on Soil Subjected to Axial Load and Biaxial Bending. II: Design Aids*. International Journal of Geomechanics. 13(2):120-131. https://doi.org/10.1061/(ASCE)GM.1943-5622.0000210

Soto-Garcia, S., Luévanos-Rojas, A., Barquero-Cabrero, J.D., López-Chavarría, S., Medina-Elizondo, M., Farias-Montemayor, O.M. and Martinez-Aguilar, C. (2022). *A New Model for the Contact Surface With Soil of Circular Isolated Footings Considering that the Contact Surface Works Partially Under Compression*. International Journal of Innovative Computing, Information and Control. 18(4):1103-1116. http://www.ijicic.org/ijicic-180406.pdf

Vela-Moreno, V.B., Luévanos-Rojas, A., López-Chavarría, S., Medina-Elizondo, M., Sandoval-Rivas, R. and Martinez-Aguilar, C. (2022), *Optimal area for rectangular isolated footings considering that contact surface works partially to compression*. Structural Engineering and Mechanics. 84(4):561-573. https://doi.org/10.12989/sem.2022.84.4.561

Velázquez-Santillán, F., Luévanos-Rojas, A., López-Chavarría, S., Medina-Elizondo, M. and Sandoval-Rivas, R. (2018), *Numerical experimentation for the optimal design for reinforced concrete rectangular combined footings*. Advances in Computational Design. 3(1):49-69. https://doi.org/10.12989/acd.2018.3.1.049

Yáñez-Palafox, J.A., Luévanos-Rojas, A., López-Chavarría, S. and Medina-Elizondo, M. (2019), *Modeling for the strap combined footings Part II: Mathematical model for design*. Steel and Composite Structures. 30(2):109-121. https://doi.org/10.12989/scs.2019.30.2.109